View metadata, citation and similar papers at core.ac.uk

brought to you by CORE

provided by Missouri University of Science and Technology (Missouri S&T): Scholars' Mine

Scholars' Mine

Doctoral Dissertations

Student Theses and Dissertations

Fall 2009

Fully differential cross sections for four-body scattering processes

Allison L. Harris

Follow this and additional works at: https://scholarsmine.mst.edu/doctoral_dissertations

 Part of the Physics Commons

Department: Physics

Recommended Citation

Harris, Allison L., "Fully differential cross sections for four-body scattering processes" (2009). *Doctoral Dissertations*. 2177.
https://scholarsmine.mst.edu/doctoral_dissertations/2177

This thesis is brought to you by Scholars' Mine, a service of the Missouri S&T Library and Learning Resources. This work is protected by U. S. Copyright Law. Unauthorized use including reproduction for redistribution requires the permission of the copyright holder. For more information, please contact scholarsmine@mst.edu.

FULLY DIFFERENTIAL CROSS SECTIONS FOR FOUR-BODY SCATTERING PROCESSES

by

ALLISON LYNN HARRIS

A DISSERTATION

Presented to the Faculty of the Graduate School of the

MISSOURI UNIVERSITY OF SCIENCE AND TECHNOLOGY

in Partial Fulfillment of the Requirements for the Degree

DOCTOR OF PHILOSOPHY

in

PHYSICS

2009

Approved by

Don H. Madison,Co-Advisor
Jerry L. Peacher, Co-Advisor
Michael Schulz
Paul E. Parris
Melanie Mormile

Copyright 2009
Allison Lynn Harris
All Rights Reserved

ABSTRACT

While the original concept of the atom can be traced back to the ancient Greeks, current knowledge of the atom is due largely to the study of atomic collisions. The structure of atoms is now fairly well understood, but the understanding of their interactions remains incomplete. In atomic collisions, the particles involved in the collision interact through the Coulomb force, which is known exactly. However, for Coulomb forces, the solution of the Schrödinger equation can only be obtained analytically for two mutually interacting particles. As a result, when more than two particles are involved, theory must resort to approximations. The validity of these approximations is then determined by comparison with experiment.

Three new fully quantum-mechanical models that include all relevant two-particle interactions are presented here, and used to study fully differential cross sections (FDCS) of four-body collisions. In particular, this work focuses on electron-impact excitation-ionization of helium, as well as single charge transfer, transfer-excitation, and double charge transfer in proton + helium collisions. The calculations required for this work result in nine-dimensional integrals that are performed numerically.

For excitation-ionization, the projectile-ejected electron interaction is found to be important in correctly predicting the shape of the FDCS. However, the projectile-atom and projectile-ion interactions play a much smaller role in this process. For single charge transfer and transfer-excitation, the current model does a reasonable job of predicting the shape and magnitude of experiment. However, for double charge transfer, the theoretical results overestimate experiment by several orders of magnitude. For all of the charge transfer collisions, calculations show that the interaction of the electrons within the target atom has little effect on the FDCS.

ACKNOWLEDGMENT

To my parents, thank you for your love, support, and encouragement, and for always inspiring me to be curious. I owe my interest in science, and physics in particular, to you. Thank you to my friends, and fellow graduate students, Tina, Ola, Aaron, and Ben for all of the great memories. Graduate school was much more fun because of you. To my extended family and friends, thanks for providing an always welcome break from the rigors of school.

Thanks, also, to my advisors, Dr. Don Madison and Dr. Jerry Peacher, for your continual patience and all that you have taught me. I am grateful for the opportunities you have provided and your willingness to share your expertise. Thank you to the faculty members who agreed to serve on my committee: Dr. Michael Schulz for the experiments that were the motivation for this work; Dr. Paul Parris for all the help along the way, and the many miles on the road; and Dr. Melanie Mormile for providing me the opportunity to broaden my horizons beyond the physics department.

Finally, thank you to everyone in the physics department for making Missouri S&T a great place to be a graduate student.

TABLE OF CONTENTS

Page

ABSTRACT iii

ACKNOWLEDGMENT iv

LIST OF ILLUSTRATIONS vii

LIST OF TABLES xi

SECTION

1. INTRODUCTION 1
   - 1.1. EXCITATION-IONIZATION 2
   - 1.2. TRANSFER-EXCITATION 5
   - 1.3. DOUBLE ELECTRON CAPTURE 10
2. THEORY 13
   - 2.1. GENERAL THEORY 13
     - 2.1.1. Potential Scattering 13
       - 2.1.1.1. Separation of the Center of Mass Motion 13
       - 2.1.1.2. The Scattering Amplitude 14
       - 2.1.1.3. Alternate Form of the Scattering Amplitude 17
     - 2.1.2. Coulomb Scattering 19
     - 2.1.3. Derivation of the T-Matrix 20
     - 2.1.4. Two Potential Formulation 28
     - 2.1.5. Differential Cross Sections 29
   - 2.2. EXCITATION-IONIZATION 32
     - 2.2.1. 4-Body Distorted Wave (4DW) Model 32
     - 2.2.2. First Born Approximation (FBA) Model 36
   - 2.3. SINGLE CHARGE TRANSFER AND TRANSFER-EXCITATION 36
     - 2.3.1. 4-Body Transfer-Excitation (4BTE) Model 37
   - 2.4. DOUBLE CHARGE TRANSFER 40
     - 2.4.1. 4-Body Double Capture (4BDC) Model 40
3. RESULTS 42
   - 3.1. EXCITATION-IONIZATION 42
     - 3.1.1. Cross Normalized Results 42
     - 3.1.2. Absolute Ratio Results 44
     - 3.1.3. Absolute Results 48

3.2. SINGLE CHARGE TRANSFER 54
3.3. TRANSFER-EXCITATION 54
3.4. DOUBLE CHARGE TRANSFER 60
4. CONCLUSION 66

APPENDICES

A. ATOMIC UNITS 70
B. CALCULATION OF THE FINAL STATE PERTURBATION 72
C. EIKONAL WAVEFUNCTION FOR TWO ACTIVE ELECTRONS 78
D. CODE TESTING 80
D.1. *4DW.F* 81
D.2. *TRANSFER.F* 81
D.3. *TRANSFER.DOUBLE.CAPTURE.F* 83

BIBLIOGRAPHY 84

VITA 93

LIST OF ILLUSTRATIONS

Figure Page

2.1 Coordinate system for the projectile-helium atom system, in which r_1, r_{12}, and r_{13} are the magnitudes of the relative coordinates of the projectile to the helium nucleus and atomic electrons respectively. 33

2.2 Jacobi coordinate system for the projectile-helium atom system. 38

2.3 Jacobi coordinate system for the hydrogen-helium ion system. 39

3.1 Theoretical FDCS for electron-impact excitation-ionization of helium as a function of ejected electron angle θ_e. Results of the 4DW, FBA, and DWB2-RMPS (divided by 1.8) models are compared to the relative experimental results of [10]. The incident energy is 500 eV. Experimental results have been normalized to the binary peak of the 4DW calculation at $E_2 = 3$ eV and $\theta_a = 4.1°$ 43

3.2 Theoretical results of the 4DW and FBA theories for FDCS ratios for excitation-ionization as a function of ejected electron angle θ_e with a scattering angle of $\theta_a = 32°$. The calculations are compared to a DWB2-RMPS calculation and absolute experimental data [8]. Incident projectile energies are: (a) $E_0 = 268.6$ eV (n = 1) and $E_0 = 309.4$ eV (n = 2); (b) $E_0 = 268.6$ eV (n = 1) and $E_0 = 316.9$ eV (n = 3); (c) $E_0 = 112.6$ eV (n = 1) and $E_0 = 153.4$ eV (n = 2); (d) $E_0 = 112.6$ eV (n = 1) and $E_0 = 161.0$ eV (n = 3). For (a) and (b), the FBA has been divided by 5, and the 4DW has been divided by 3. For (c) and (d), the FBA has been divided by 5, and the 4DW has been divided by 2. 46

3.3 Theoretical results of the 4DW and FBA models for FDCS ratios for excitation-ionization as a function of ejected electron angle θ_e for a scattered projectile energy of 150 eV and an ionized electron energy of 20 eV. The calculations are again compared to a DWB2-RMPS calculation and absolute experimental data [8]. For panel (a), the 4DW and FBA have been divided by 2.5. For panel (b) the 4DW and FBA have been divided by 5, and the DWB2-RMPS has been divided by 2. All other calculations are absolute. 47

3.4 Comparison of theoretical calculations for ionization without excitation as a function of ejected electron angle θ_e with a scattering angle of $\theta_a = 32°$. The incident energies are (a) $E_0 = 268.6$ eV and (b) $E_0 = 112.6$ eV.. 49

3.5 Comparison of theoretical calculations for ionization without excitation as a function of ejected electron angle θ_e with an incident energy of $E_0 = 194.6$ eV and an ejected electron energy of $E_2 = 20$ eV. 50

3.6 Absolute FDCS as a function of ejected electron angle θ_e with a scattering angle of $\theta_a = 32°$. The 4DW and FBA theories are compared to the DWB2-RMPS model and "absolute experimental" results [8]. The FBA and 4DW calculations have been multiplied by 2 and 2.5 in (a) and (b) respectively. Incident energies are the same as those listed for figure 3.2. . 51

3.7 Absolute FDCS as a function of ejected electron angle θ_e with a scattered projectile energy of 150 eV and an ejected electron energy of 20 eV. The 4DW and FBA theories are compared to the DWB2-RMPS model and "absolute experimental" results [186]. The FBA and 4DW calculations have been multiplied by 2 for the n = 2 results and by 2.5 for the n = 3 results. 52

3.8 FDCS as a function of projectile scattering angle for p + He SC. Experiment: ■ results of Schulz et al. [172] for the incident projectile energies shown in the figure. Both theoretical curves are from the 4BTE model with a plane wave for the incident projectile, Hylleraas wave function for the helium atom, and a Coulomb wave for the scattered projectile. Theoretical results: — all three terms in the perturbation; - - - no projectile-nuclear term in the perturbation. 55

3.9 FDCS as a function of projectile scattering angle for p + He TE showing the relative magnitudes of excitation to different energy levels in the He^+ ion. All theoretical curves are from the 4BTE model with a plane wave for the incident projectile, Hylleraas wave function for the helium atom, and Coulomb wave for the scattered projectile. Theoretical results: — excitation to the n = 2 level; - - - excitation to the n = 3 level; $\cdots$ excitation to the n = 4 level. 56

3.10 FDCS as a function of projectile scattering angle for p + He TE showing the effect of the incident projectile-target atom interaction. Experiment: ■ results of Hasan et al. [168] for the incident projectile energies shown in the figure. Theoretical results: — 4BTE model with an Eikonal wave function for the incident projectile, Hylleraas wave function for the helium atom, and plane wave for the scattered projectile; - - - 4BTE model with a plane wave for the incident projectile, Hylleraas wave function for the helium atom, and plane wave for the scattered projectile 57

3.11 FDCS as a function of projectile scattering angle for p + He TE showing the effect of the incident projectile-target atom interaction. Experiment: ■ results of Hasan et al. [168] for the incident projectile energies shown in the figure. Theoretical results: — 4BTE model with an Eikonal wave function for the incident projectile, Hylleraas wave function for the helium atom, and Coulomb wave for the scattered projectile; - - - 4BTE model with a plane wave for the incident projectile, Hylleraas wave function for the helium atom, and Coulomb wave for the scattered projectile. 58

3.12 FDCS as a function of projectile scattering angle for p + He TE showing the effect of the scattered projectile-residual ion interaction. Experiment: ■ results of Hasan et al. [168] for the incident projectile energies shown in the figure. Theoretical results: — 4BTE model with a plane wave for the incident projectile, Hylleraas wave function for the helium atom, and Coulomb wave for the scattered projectile; - - - 4BTE model with a plane wave for the incident projectile, Hylleraas wave function for the helium atom, and plane wave for the scattered projectile. 59

3.13 FDCS as a function of scattering angle for p + He TE showing the effect of electron correlation in the target atom wave function. Experiment: ■ results of Hasan et al. [168] for the incident projectile energies shown in the figure. Theoretical results: — 4BTE model with a plane wave for the incident projectile, Hylleraas wave function for the helium atom, and Coulomb wave for the scattered projectile; - - - 4BTE model with a plane wave for the incident projectile, Hartree-Fock wave function for the helium atom, and Coulomb wave for the scattered projectile. 60

3.14 FDCS as a function of scattering angle for p + He TE showing the effect of the projectile-nuclear interaction. Experiment: ■ results of Hasan et al. [168] for the incident projectile energies shown in the figure. Both theoretical curves are from the 4BTE model with a plane wave for the incident projectile, Hylleraas wave function for the helium atom, and Coulomb wave for the scattered projectile. Theoretical results: — all three terms in the perturbation; - - - without the projectile-nuclear term in the perturbation. 61

3.15 FDCS as a function of projectile scattering angle for p + He DC. Experiment: ■ results of Schulz et al. [172] for the incident projectile energies shown in the figure. Both theoretical curves are from the 4BTE model with a plane wave for the incident projectile, Hylleraas wave functions for the helium atom and H^- ion, and a Coulomb wave for the scattered projectile. Theoretical results: — all three terms in the perturbation; - - - without the projectile-nuclear term in the perturbation. Both calculations have been divided by 100. 62

3.16 FDCS for 75 keV p + He DC showing the effect of electron correlation in the target atom and the scattered ion. Experiment: ■ results of Schulz et al. [172]. All calculations are the 4BTE model with a plane wave for the incident projectile and Coulomb wave for the scattered projectile. The labels in the figure indicate the helium atom and H^- wave functions respectively. All calculations have been divided by 100. 63

3.17 FDCS ratios for p + He DC divided by p + He SC. Experiment: ■ results of Schulz et al. [172] for the incident projectile energies shown in the figure. Both theoretical curves are from the 4BTE model with a plane wave for the incident projectile, Hylleraas wave functions for the helium atom and H^- ion, and a Coulomb wave for the scattered projectile. Theoretical results: — all three terms in the perturbation divided by (a) 100, (b) 35, (c) 25; - - - without the projectile-nuclear term in the perturbation divided by 10 in all three panels. 64

LIST OF TABLES

Table Page

D.1 Results of analytic code checking for *transfer.f* code. 82

D.2 Results of numerical code checking for *transfer.f* code. 83

1. INTRODUCTION

Atomic collisions have been studied since the early 20^{th} century and have played a crucial role in the development of physics. Beginning with the well-known experiment by Geiger and Marsden [1], and corresponding calculation by Rutherford [2], atomic collisions have been used to study the structure and interactions of atoms. Aside from this purely scientific endeavor, atomic collisions also have many important applications, including astrophysics, plasma physics, and biophysics.

Atomic collisions is a broad field of study, and the work presented here falls into the narrow subset of four-body problems. In general, the four-body problem will be defined as any collision involving the interaction of four atomic particles (i.e. electrons, protons, nuclei and/or their antiparticles). One of the simplest four-body problems is that of a single charged particle interacting with a two-electron atom or ion. The possible outcomes of such a collision include excitation-ionization, double excitation, and double ionization for either positively or negatively charged projectiles, as well as single charge transfer, double charge transfer, transfer-excitation, and transfer-ionization for positively charged projectiles. Other four-body collisions include charged particle collisions with molecules, as well as atom-atom collisions. This work will focus on excitation-ionization, transfer-excitation, and double charge transfer.

For charged particles interacting through the Coulomb force, the motions of the particles can only be described exactly for two particles. To describe the motion of three or more mutually interacting particles, some approximation must be made. Much work has been done on the three-body problem, and agreement between experiment and theory is quite good for simple atoms [3–6]. A natural next step is to extend the three-body models to four-body models. This has not been a simple task, and current four-body models do not yet provide an accurate description of the physical

process. In an effort to advance the overall understanding of four-body processes, new theoretical models are presented here for the study of four specific reactions.

1.1. EXCITATION-IONIZATION

The first collision process to be discussed is electron impact excitation-ionization of helium (hereafter referred to as EI). In EI, an incident electron collides with a helium atom, causing one of the atomic electrons to be ionized and the other to be promoted to an excited state of the ion. Over the last two decades, several experimental and theoretical studies have been conducted for this process. A wide range of kinematical conditions have been measured experimentally [7–13], and a number of theories have been developed to examine how different treatments of the particles and their interactions affect the fully differential cross sections (FDCS). A cross section is considered fully differential if the position and momenta of all initial and final state particles is known. The following is a summary of the existing theoretical models for excitation-ionization, and some of the conclusions drawn from them [14].

Several models explore the role of the ground state helium atom wave function, and the choice of this wave function has been shown to change both the magnitude and shape of the FDCS [8, 15]. In particular, Balashov and Bodrenko [15] examined the difference between a six parameter Hylleraas wave function and a 41 parameter wave function by Tweed [16]; Dupré et al. [9] compared a Hartree-Fock wave function and a multi-channel close-coupling wave function; and Bellm et al. [8] compared a 20 parameter Hylleraas wave function with the Pluvinage wave function. All of these results show that there is little difference in the FDCS for the various wave functions when the He^+ ion is left in the ground state, but drastically different results when the ion is left in an excited state. These calculations also show that it is important to use a wave function that contains both radial and angular electron correlations.

Correlation is defined as the mutual interaction of the atomic electrons in the initial state.

Besides correlation in the ground state helium atom wave function, correlation between the two outgoing electrons in the final state could also be important in the EI process. Franz and Altick [17] explicitly included the Coulomb interaction between the two outgoing electrons in their final state wave function, and found improved agreement with experiment. Kheifets et al. [11] also found improved agreement when including final state correlations using a coupled-channel approach. In both cases, the inclusion of additional correlation in the final state wave function produced a shift toward smaller angles in the recoil peak and larger angles in the binary peak [11,17,18], which is consistent with what one would expect from the mutual repulsion of the two electrons. The recoil peak is a result of the electron being ejected in the backward direction, and the the binary peak is a result of the electron being ejected in the forward direction. The results of Franz and Altick [17] and Kheifets et al. [11] show that an accurate prediction of the location of the binary and recoil peak requires the inclusion of final state correlations.

Obviously, the ejected electron is an active participant in these final state correlations, and several different treatments of the ejected electron-He^+ ion interaction also have been explored. Dupré et al. [9] used an orthogonalized Coulomb wave in the field of the residual ion; Franz and Altick [17,19], Chen and Madison [20], and Bellm et al. [8] used a Hartree-Fock distorted wave; Kheifets et al. [11, 21], Marchalant et al. [12, 22], Balashov and Bodrenko [15], and Sakhelashvili et al. [10] used a close-coupling approach; and Kheifets et al. [21], Fang and Bartschat [23], Sakhelashvili et al. [10], and Bellm et al. [7, 8] used an R-Matrix treatment. It is important to point out that the close-coupling and R-Matrix treatments of the ejected electron should yield the same results, as long as both of the expansions have converged [21]. However, when relatively few states are used in the expansion, significant discrepancies

exist between the two methods, with more states leading to better results [11]. For larger ejected electron energies, all of these methods yield similar results, but discrepancies appear when the energy of the ejected electron becomes less than about 10 eV. Currently, there is no single treatment of the ejected electron that leads to satisfactory agreement with experiment for all of the measurements.

Most of the models mentioned above would typically be called first order theories, meaning that they are first order in the perturbation. The sensitivity of the FDCS to changes in the initial and final state wave functions for these first order treatments suggests that a second order theory may be needed to more accurately treat this problem [9, 24]. Several second order theories have been developed, including calculations by Franz and Altick [19], Marchalant et al. [12], Fang and Bartschat [23], Sakhelashvili et al. [10], Chen and Madison [20], and Bellm et al. [7, 8].

The first thing to note about the second order theories is that they all result in improved agreement with experiment over their analogous first order counterparts. This is to be expected since two interactions are required to get two atomic electrons to change state, implying that a second order theory should be better. The second thing to note is that all second order theories produce an increase in the recoil peak compared to the corresponding first order theories.

It should be pointed out that the terms 'first order' and 'second order' can be misleading if not properly defined. All of the previous 'first order' calculations include the interaction between the projectile electron and the two atomic electrons to first order, and similarly, all of the second order theories include this interaction to second order. However, it is possible to have a first order model that includes certain interactions to higher order. For example, any physics contained in the wave function is automatically treated to all orders of perturbation theory.

While the inclusion of second order effects in the calculations does improve agreement with experiment, there are still large discrepancies between experiment

and theory. In particular, the second order theories do not predict the proper angular location for the binary and recoil lobes [10, 12, 20, 22], and there are problems with the shape and absolute magnitude of the FDCS [12, 20, 22].

1.2. TRANSFER-EXCITATION

The second collision process to be discussed is charge transfer in proton + helium collisions with simultaneous excitation of the He^+ ion (hereafter referred to as transfer-excitation, TE). Here, an incident proton collides with a helium atom, captures a single electron, and leaves the collision as a neutral ground state hydrogen atom. The remaining electron in the He^+ ion is left in an arbitrary excited state. Unlike the EI, TE will occur only with a positively charged projectile, typically a proton or other heavy ion.

The specific process of TE has been studied very little, but the similar process of charge transfer without excitation (or single capture, SC) has been studied a great deal [25–164], typically in the form of total cross sections. Both single and double charge transfer (discussed in the next section) have applications for plasmas [43, 165], low wavelength lasers [165], stellar atmospheres, proton auroras [47], and most commonly thermonuclear fusion [43–46, 165].

The first theoretical model for charge transfer was developed by Thomas [25] in 1927 for alpha particle collisions with hydrogen, and was strictly a classical calculation. Thomas's model for charge transfer consisted of a two-step process. The first step is a close collision between the projectile and the bound electron. This causes the electron to scatter towards the nucleus with the speed of the incident projectile. The second step is a close collision between the electron and the target nucleus, sending the electron out in the same direction, and with the same speed, as the scattered projectile, resulting in capture. This mechanism leads to the presence of what is now known as the Thomas peak in the differential cross section.

The year after Thomas's calculation, Oppenheimer [26] performed the first quantum mechanical calculation for charge transfer, followed two years later by Brinkman and Kramers [29]. Their model would later become known as the OBK approximation. In the OBK approximation, the projectile is treated as a plane wave in both the initial and final states, and only the interaction between the projectile and the atomic electron is included. The projectile-nuclear interaction is ignored based on the assumption that this term only contributes due to the nonorthogonality of the initial and final state wave functions [26]. The OBK calculation yielded results that were at least a factor of four too large [30], and nearly fifteen years passed before Jackson and Schiff [30] (hereafter referred to as JS) performed a calculation using the full interaction potential, including the projectile-nuclear term.

The JS results agreed with experiment much better than the OBK results, and correctly predicted the magnitude [30, 48] of the cross section. Since the OBK and JS models were introduced, much discussion has centered around the inclusion of the projectile-nuclear term. It has been shown by Belkić and Salin [34] that including the projectile-nuclear term in the perturbation improves agreement with experiment, particularly at large angles. When this interaction is ignored, the differential cross section drops off much more quickly than when it is included. This can be attributed to the idea that scattering of the projectile through a large angle is typically a result of scattering from the nucleus. Classically, this is analogous to small impact parameter scattering, where the projectile penetrates the electron cloud, and scatters elastically from the nucleus. It is now accepted that the projectile-nuclear term in the perturbation needs to be included to accurately predict the magnitude of the charge transfer cross section.

For single charge transfer, the use of hydrogen as a target is clearly the simplest case to study, and it was nearly 30 years after Thomas's proton + hydrogen calculation before a calculation was done with a helium target. For helium, the problem can still

be treated as a three-body process if it is assumed that the non-captured electron is passive, and only serves to screen the nuclear charge. The first calculation for charge transfer from helium was performed by Bransden, Dalgarno, and King [35] in 1954, using the OBK approximation.

From this time forward, calculations for capture from helium were performed almost exclusively using the independent electron model [35, 49–67]. In this model, the two target electrons are treated independently, and no interaction between them is included in the calculation. The few exceptions to this are a 1963 paper by Mapleton [37], and a 1987 paper by Crothers and McCarroll [68]. The Mapleton paper uses a six parameter Hylleraas wave function for the target helium atom, which includes electron-electron correlation. Mapleton found that compared to a variational helium wave function with no correlation, total cross sections calculated with a Hylleraas wave function were smaller, particularly in the OBK approximation at high energy. Crothers and McCarroll used a Pluvinage wave function, and similarly found that including correlation lowered the magnitude of the total cross section.

The advances that were made within the independent electron model typically involved the treatment of the projectile-target interaction. One such model is the Continuum Distorted Wave (CDW) model, which includes the long-range Coulomb interaction between the projectile and the captured electron in the initial state [70]. It also includes continuum intermediate states that satisfy the correct boundary conditions [134].

Another common treatment of the projectile-target interaction is the Eikonal approximation, which includes the distortion of the incident projectile wave function due to the target through the inclusion of a phase factor. Other models include the Static Brinkman-Kramers [50], Coulomb Brinkman-Kramers [71, 72], Binary Encounter [56, 73], Distorted Wave Born [40, 58, 74–76], Boundary Corrected First Born [80–84, 166], Second Born [61, 62, 89–104], Strong Potential Born [77–79],

Coulomb Born [83, 86, 88], and the Born Distorted Wave [63, 85] approximations. All are different approximations for treating the Coulomb boundary conditions. It has been shown that neglect of Coulomb boundary conditions results in large discrepancies between experiment and theory [38, 39, 82].

Within the three-body model, it is also possible to have capture to an excited state, where the outgoing hydrogen atom is in an excited state. Oppenheimer [26] was the first to show that total cross sections for capture to an excited state scale as n^{-3}. Thus, the cross section for capture to any state is simply 1.2 times the cross section for capture to the ground state.

Most of the work done for charge transfer has involved total cross sections. A much more stringent test of theory is the study of cross sections that are differential in projectile scattering angle. For proton + hydrogen single charge transfer, the first differential cross section calculations were performed by Bassel and Gerjuoy [40] in 1960. For proton + helium single charge transfer, differential cross sections were not calculated until the late 1970s [50, 51]. In both cases, the collision was treated as a three-body problem, with only the captured electron taking part in the reaction. A very recent paper by Schöffler et al. [167] included electron correlation in the target atom wave function, and found that the differential cross section is unaffected by the inclusion of correlation.

In general, differential cross sections for proton + helium single charge transfer decrease rapidly as the scattering angle increases, and typically exhibit a change in slope between a scattering angle of 0.03° and 0.08°. This change in slope represents the boundary between small and large angle scattering. At small angles, the projectile scattering is a result of scattering from the atomic electrons, whereas for large angles, it is a result of nuclear scattering, as discussed above [51].

Relatively early in the theoretical study of charge transfer, second order calculations were performed [41,42,61,62,89–104]. For total cross sections, the second order

terms were, surprisingly, the same magnitude as the first order terms. In fact, at projectile energies above a few MeV, the second order term dominates [89,91,92,98,104]. It has also been shown that the second order contributions become more important as the charge of the target nucleus increases [95]. For differential cross sections, first order theories predict a zero in the FDCS, but inclusion of second order terms removes this zero. At high energies, second order theories also introduce a peak in the differential cross section at 0.5° corresponding to the Thomas mechanism. This is not surprising since the two-step Thomas process should require a second order theory for an adequate description.

In terms of projectile speed (or equivalently projectile energy), charge transfer collisions generally divide into three regimes. The first involves collisions with a projectile speed less than one atomic unit[1]. For this case, it is common to use a two center molecular orbital approach. At the other end of the energy spectrum are collisions with relativistic projectile speeds. The range in between is typically referred to as the intermediate energy range, and for proton projectiles is about 25 keV to 2 MeV.

While TE is a similar process to SC, it presents additional theoretical challenges due to all four particles being actively involved in the collision. A theoretical treatment of this process requires a full four-body model, and to date there is only one existing model due to Kirchner [168, 169]. Kirchner's model is a semi-classical, non-perturbative impact parameter model that uses the independent electron model. It has shown that electron correlation in the target atom is not important in predicting the structure of the ratio of transfer-excitation times single excitation divided by single capture times double excitation. This structure is attributed to a quantum mechanical treatment of the projectile scattering. Experimental absolute differential

[1] 1 a.u. of speed corresponds to the speed of an electron in the first Bohr orbit of hydrogen.

cross sections for TE show little structure themselves, while Kirchner's theory predicts some structure. This predicted structure is not unique to the TE process, but also occurs in single-transfer calculations [63, 66] where experiment again shows little structure.

1.3. DOUBLE ELECTRON CAPTURE

A process similar to single charge transfer and TE is that of double charge transfer (or double capture, DC). It is the fourth collision process studied here, again within the context of proton + helium collisions. In DC, the incident proton captures both atomic electrons from the target helium atom and leaves the collision as an H^- ion. DC was first studied in the mid-to-late 1960s, but the vast majority of work on this problem has been completed in the last 30 years. This is due mostly to the difficulty of treating a full four-body problem, and the fact that DC cross sections are typically 2 to 3 orders of magnitude smaller than SC, making measurement and calculation difficult.

Like single capture, most work on DC has involved total cross sections, and typically the resonant process of alpha particles, or more highly charged bare projectiles, incident on helium atoms. In these cases, DC to excited states is not small compared to DC to the ground state [46, 106–108]. Thus, any calculation performed would need to include capture to excited states in order to accurately compare with experiment. In the case of proton collisions, the electrons are guaranteed to be captured to the ground state because the H^- ion has no stable excited states. This greatly reduces the amount of computation required.

Many theories have been applied to the DC process, and generally they are the same theories used for the SC process (i.e. the Close Coupling Approximation, Classical Trajectory Monte Carlo, Two State Atomic Expansion, Coulomb Distorted Wave,

OBK, Time-Dependent Hartree-Fock, Boundary Corrected First Born, Coulomb Distorted Wave-Eikonal Initial State, and 4-Body Coulomb Distorted Wave). In DC, the main focus of many of these studies is the role of electron-electron correlation. Initially the independent electron (particle) model was used in order to simplify the calculation [170]. In this model, any contribution to the DC cross section resulting from one electron being captured due to its interaction with the other is ignored [109]. The independent electron model is typically valid for high target nuclear charge [110], and high incident projectile velocity [105], where correlation is not important. However, since this is a true four-body problem, one would expect that some correlation should be included.

The next step theoretically was the independent event model. In this model, static correlation is included in the target wave function, but generally dynamic correlation is not included. Dynamic correlation involves the inclusion of the Coulomb interaction between the final state captured electron and the residual ion, and should result in structure in the differential cross section similar to a Thomas peak in SC [111]. Within these models, the probability of a two electron transition is approximated as the product of two single electron transitions. The independent event model considers DC to be the result of two successive single capture events [112].

Both the independent particle model and the independent event model ignore any four-body effects which may be present. This spurred the development of several full four-body models [43, 68, 109, 111, 171], all of which found that correlation had little effect on the total or differential cross section. The inclusion of correlation generally decreased the cross section by less than a factor of 3, but did not alter the shape.

The first differential DC cross section was calculated in 1991 by Schuch et al. [111] for α + helium resonant capture. Since then, only four other calculations of differential cross sections for DC have been performed, all for α + helium collisions.

Schuch et al. [111] and Gravielle and Miralglia [113] showed that electron correlation is not very important; Belkić [114] showed that the Boundary Corrected First Born approximation has a zero in the differential cross section at 0.112 mrad due to the potential vanishing at this scattering angle; Schöffler et al. [167] found a minimum in the DC cross section similar to that in the SC cross section when using the Born Distorted Wave model; and Martínez [106] showed that a double peak structure due to a double scattering mechanism is observed when the energy is large enough.

At this point, only three sets of experimental differential cross section results exist for non-resonant DC, and there is only one theoretical model. The experimental results are those of Schulz et al. [172] for proton + helium, and Martinez et al. [173] and Afrosimov et al. [174] for proton + argon. The theoretical results are those of Martinez et al. [173] for proton + argon. Thus, the work presented here represents the first theoretical differential cross sections for proton + helium DC.

2. THEORY

2.1. GENERAL THEORY

The goal of any atomic collision experiment is to study a fundamentally quantum mechanical process. From a theoretical perspective, the study of atomic collisions amounts to solving the Schrödinger equation for a particular Hamiltonian with particular boundary conditions[2]. The basic elements of scattering theory are presented in this section, and atomic units[3] are used throughout, unless otherwise noted.

2.1.1. Potential Scattering.

2.1.1.1. Separation of the Center of Mass Motion. Consider the interaction of two non-relativistic, spinless, charged particles, A and B, with masses m_A and m_B, coordinates $\vec{r}_A$ and $\vec{r}_B$, and momenta $\vec{p}_A$ and $\vec{p}_B$. Assuming that the interaction potential depends only on the relative distance $r = \mid \vec{r}_A - \vec{r}_B \mid$ between A and B, the corresponding Hamiltonian is

$$H = \frac{-1}{2m_A}\nabla_A^2 + \frac{-1}{2m_B}\nabla_B^2 + V(r). \tag{1}$$

The center of mass vector for A and B is defined as

$$\vec{R} = \frac{m_A\vec{r}_A + m_B\vec{r}_B}{M}, \tag{2}$$

where $M = m_A + m_B$. Using equation (2) and the relative coordinate $\vec{r}$, the Hamiltonian from equation (1) can then be written as

$$H = \frac{-1}{2M}\nabla_R^2 + \frac{-1}{2\mu}\nabla_r^2 + V(r), \tag{3}$$

where $\mu = m_A m_B/(m_A + m_B)$ is the reduced mass.

[2]The derivations in this section closely follow those of [175].

[3]See Appendix A for a list of atomic units.

Now, the wave function satisfying Schrödinger's equation for the Hamiltonian in equation (3) can be written as

$$\Psi(\vec{R},\vec{r}) = \chi(\vec{R})\phi(\vec{r}), \tag{4}$$

where $\chi(\vec{R})$ is the wave function for the center of mass motion, and $\phi(\vec{r})$ is the wave function for the relative motion of A and B. These wave functions satisfy

$$\frac{-1}{2M}\nabla_R^2\chi(\vec{R}) = E_{CM}\chi(\vec{R}) \tag{5}$$

and

$$\left[\frac{-1}{2\mu}\nabla_r^2 + V(r)\right]\phi(r) = E_{rel}\phi(r). \tag{6}$$

The total energy can then be written as $E = E_{CM}+E_{rel}$. Because the center of mass of the system is moving at a constant velocity, a transformation to the reference frame where the origin is located at the center of mass can be made. This allows for the motion of the center of mass to be neglected, and only solutions to equation (6) are needed.

2.1.1.2. The Scattering Amplitude. Since $V(r)$ does not depend on time, the eigenstates of the Schrödinger equation can be written as

$$\Psi(\vec{r},t) = \psi(\vec{r})e^{-iE_{rel}t}, \tag{7}$$

where the total kinetic energy in the center of mass frame can be expressed as $E_{rel} = k^2/2\mu$. Note that, $k_i = k_f = k$ for potential scattering, where $\vec{k}_i$ is the incident wavevector and $\vec{k}_f$ is the scattered wavevector. Thus, the time-independent Schrödinger equation can be written as

$$H\psi(\vec{r}) = E_{rel}\psi(\vec{r}). \tag{8}$$

Applying the substitution $U(r) = 2\mu V(r)$ gives the following differential Schrödinger equation

$$\left[\nabla_r^2 + k^2 - U(r)\right] \psi(\vec{r}) = 0. \tag{9}$$

The solution to this equation must asymptotically satisfy the following boundary condition[4] for large r

$$\begin{aligned} \psi(\vec{r}) &\rightarrow \psi_I + \psi_{SC} \\ &\rightarrow N\left[e^{i\vec{k}_i\cdot\vec{r}} + \frac{e^{ikr}}{r} f(k,\theta,\varphi)\right], \end{aligned} \tag{10}$$

where the first term represents an incoming plane wave and the second term is an outgoing spherical wave that has been scattered from the target. The quantity N is a normalization constant, and θ and φ are spherical polar coordinates corresponding to the direction $\hat{k}_f$. The function $f(k,\theta,\varphi)$ is known as the scattering amplitude, and its determination yields the complete solution to the Schrödinger equation.

To find an expression for $f(k,\theta,\varphi)$, it is useful to write equation (9) in integral form. Rearranging equation (9) and putting in the explicit wavevector dependence gives

$$\left[\nabla_r^2 + k^2\right] \psi_{\vec{k}_i}(\vec{r}) = U(r)\psi_{\vec{k}_i}(\vec{r}), \tag{11}$$

where the term on the right hand side can now be considered an inhomogeneous source term. The general solution to this equation is

$$\psi_{\vec{k}_i}(\vec{r}) = \beta_{\vec{k}_i}(\vec{r}) + \int G_0(k,\vec{r},\vec{r}\,')U(r')\psi_{\vec{k}_i}(\vec{r}\,')d^3r', \tag{12}$$

[4]This solution holds only for potentials that approach zero faster than r^{-1}, i.e. not the Coulomb potential.

which is known as the Lippmann-Schwinger equation. The term $\beta_{\vec{k}_i}(\vec{r})$ is a solution to the homogenous equation $[\nabla_r^2 + k^2]\,\beta_{\vec{k}_i}(\vec{r}) = 0$. It is simply a plane wave given by

$$\beta_{\vec{k}_i}(\vec{r}) = \frac{e^{i\vec{k}_i\cdot\vec{r}}}{(2\pi)^{3/2}}, \tag{13}$$

and $G_0(k, \vec{r}, \vec{r}\,')$ is the Green's function satisfying

$$\left[\nabla_r^2 + k^2\right] G_0(k, \vec{r}, \vec{r}\,') = \delta(\vec{r} - \vec{r}\,'). \tag{14}$$

To determine the Green's function, it is useful to write the Dirac delta function in its integral form,

$$\delta(\vec{r} - \vec{r}\,') = \frac{1}{(2\pi)^3}\int e^{i\vec{k}'\cdot(\vec{r}-\vec{r}\,')}d^3k'. \tag{15}$$

It is also helpful to introduce the Fourier transform of the Green's function $g_0(k, \vec{k}', \vec{r}\,')$ so that $G_0(k, \vec{r}, \vec{r}\,')$ can be written as

$$G_0(k, \vec{r}, \vec{r}\,') = \frac{1}{(2\pi)^3}\int g_0(k, \vec{k}', \vec{r}\,')e^{i\vec{k}'\cdot\vec{r}}d^3k'. \tag{16}$$

The explicit form of $g_0(k, \vec{k}', \vec{r}\,')$ is

$$g_0(k, \vec{k}', \vec{r}\,') = \frac{e^{-i\vec{k}'\cdot\vec{r}\,'}}{k^2 - k'^2}. \tag{17}$$

By combining equations (16) and (17) and performing the appropriate integrals in the complex plane, the Green's function corresponding to the correct asymptotic boundary condition (10) is found to be

$$G_0^{(+)}(k, \vec{r}, \vec{r}\,') = -\frac{1}{4\pi}\frac{e^{ik|\vec{r}-\vec{r}\,'|}}{|\,\vec{r} - \vec{r}\,'\,|}, \tag{18}$$

where the $(+)$ denotes the outgoing wave nature.

It is now necessary to compare the asymptotic form of equation (12) with equation (10). The asymptotic form of equation (12) for an outgoing spherical wave is given by

$$\psi^{(+)}_{\vec{k}_i}(\vec{r}) \rightarrow \frac{e^{i\vec{k}_i\cdot\vec{r}}}{(2\pi)^{3/2}} - \frac{1}{4\pi}\frac{e^{ikr}}{r}\int e^{-i\vec{k}_f\cdot\vec{r}\,'}U(r')\psi^{(+)}_{\vec{k}_i}(\vec{r}\,')d^3r'. \tag{19}$$

By comparing equations (19) and (10), and using $U(r) = 2\mu V(r)$, the scattering amplitude can now be written as

$$f(k,\theta,\varphi) = -\frac{(2\pi)^{3/2}}{4\pi}\int e^{-i\vec{k}_f\cdot\vec{r}\,'}U(r')\psi^{(+)}_{\vec{k}_i}(\vec{r}\,')d^3r' \tag{20}$$

$$= -(2\pi)^2\mu\langle\beta_{\vec{k}_f} \mid V \mid \psi^{(+)}_{\vec{k}_i}\rangle, \tag{21}$$

which clearly represents the amplitude for a transition from a state $\psi^{(+)}_{\vec{k}_i}$ to $\beta_{\vec{k}_f}$ through the interaction V.

2.1.1.3. Alternate Form of the Scattering Amplitude. The form of the scattering amplitude in equation (21) is not the only representation. An alternate integral representation of the scattering amplitude can also be derived by writing the Lippmann-Schwinger equation (12) as

$$\psi^{(+)}_{\vec{k}_i}(\vec{r}) = \beta_{\vec{k}_i}(\vec{r}) + \psi^{(+)}_{sc}(\vec{r}), \tag{22}$$

where the solution to the homogenous equation $\beta_{\vec{k}_i}(\vec{r})$ is again given by equation (13), and $\psi^{(+)}_{sc}(\vec{r})$ satisfies the inhomogeneous equation

$$\left[\nabla^2_r + k^2 - U(r)\right]\psi^{(+)}_{sc}(\vec{r}) = U(r)\,\beta_{\vec{k}_i}(\vec{r}). \tag{23}$$

Let $G^{(+)}(k,\vec{r},\vec{r}\,')$ be the total Green's function that satisfies the equation

$$\left[\nabla_r^2 + k^2 - U(r)\right] G^{(+)}(k,\vec{r},\vec{r}\,') = \delta(\vec{r}-\vec{r}\,'). \tag{24}$$

Then, the outgoing spherical wave can be written as

$$\psi_{sc}^{(+)}(\vec{r}) = \int G^{(+)}(k,\vec{r},\vec{r}\,')U(r')\beta_{\vec{k}_i}(\vec{r}\,')d^3r'. \tag{25}$$

In terms of Dirac notation, equation (12) can be written as

$$\mid \psi_{\vec{k}_i}^{(+)}\rangle = \mid \beta_{\vec{k}_i}\rangle + G_0^{(+)}U \mid \psi_{\vec{k}_i}^{(+)}\rangle. \tag{26}$$

Noting that $G_0^{(+)}$ and $G^{(+)}$ are related by

$$G^{(+)} = G_0^{(+)}\left(1 + UG^{(+)}\right), \tag{27}$$

the combination of equations (22) and (25) gives

$$\mid \psi_{\vec{k}_i}^{(+)}\rangle = \mid \beta_{\vec{k}_i}\rangle + G^{(+)}U \mid \beta_{\vec{k}_i}\rangle. \tag{28}$$

Recall that this is the wave function corresponding to an incident plane wave plus an outgoing spherical wave with incident projectile wavevector $\vec{k}_i$. Then, substitution of equation (28) into the scattering amplitude (21) gives

$$f(k,\theta,\varphi) = -2\pi^2\langle\beta_{\vec{k}_f} \mid \left[U + UG^{(+)}U\right] \mid \beta_{\vec{k}_i}\rangle. \tag{29}$$

It is now useful to note that the eigenfunction of H corresponding to an incident plane wave plus an incoming spherical wave with scattered projectile wavevector

$\vec{k}_f$ is given by

$$| \psi^{(-)}_{\vec{k}_f} \rangle = | \beta_{\vec{k}_f} \rangle + G^{(-)} U \mid \beta_{\vec{k}_f} \rangle, \tag{30}$$

where

$$G^{(-)} = G^{(+)\dagger}. \tag{31}$$

Writing equation (29) as two terms, and substituting the adjoint of equation (30) into the second term gives

$$f(k, \theta, \varphi) = -2\pi^2 \langle \psi^{(-)}_{\vec{k}_f} \mid U \mid \beta_{\vec{k}_i} \rangle \tag{32}$$

$$= -4\pi^2 \mu \langle \psi^{(-)}_{\vec{k}_f} \mid V \mid \beta_{\vec{k}_i} \rangle \tag{33}$$

Equations (21) and (33) are two alternative forms for the scattering amplitude. The form given by equation (21) contains a plane wave representation for the scattered projectile, and an *outgoing* spherical wave for the incoming projectile, with the interaction between the two particles represented by V. On the other hand, the form given by equation (33) contains a plane wave representation for the incident particle, an *incoming* spherical wave for the scattered projectile, and the same interaction V between the two particles.

2.1.2. Coulomb Scattering. It was mentioned that the boundary condition of equation (10) only holds for potentials approaching zero faster than r^{-1}. The question remains of what to do in the case of Coulomb scattering, where

$$V \sim \frac{1}{r}. \tag{34}$$

By writing the Schrödinger equation for a Coulomb potential in parabolic coordinates, the solution can then be written as

$$\psi_{cw}\left(\vec{r}\right) = \frac{e^{-\pi\gamma/2}}{(2\pi)^{3/2}} e^{i\vec{k}\cdot\vec{r}} \Gamma\left(1+i\gamma\right)_1 F_1(-i\gamma, 1; ikr - i\vec{k}\cdot\vec{r}), \tag{35}$$

where ${}_1F_1(-i\gamma, 1; ikr - i\vec{k}\cdot\vec{r})$ is a confluent hypergeometric function and $\Gamma\left(1+i\gamma\right)$ is the gamma function. This solution is known as a Coulomb wave. The quantity γ is the Sommerfeld parameter, and is given by

$$\gamma = \frac{Z_A Z_B}{v}, \tag{36}$$

where Z_A and Z_B are the charges of the two particles, and v is their relative speed. The asymptotic form of the Coulomb wave can be written to first order as

$$\psi_{cw}\left(\vec{r}\right) \to \frac{1}{(2\pi)^{3/2}} \left[e^{ikz} e^{i\gamma \log\left(kr - \vec{k}\cdot\vec{r}\right)} + f_{cw}\left(\theta\right) \frac{e^{ikr} e^{-i\gamma\log(2kr)}}{r} \right], \tag{37}$$

where

$$f_{cw}\left(\theta\right) = -\gamma \frac{\Gamma\left(1+i\gamma\right)}{\Gamma\left(1-i\gamma\right)} \frac{e^{-i\gamma\log\left(\sin^2\frac{\theta}{2}\right)}}{2k\sin^2\frac{\theta}{2}}. \tag{38}$$

This can again be interpreted as an incident plane wave plus an outgoing spherical wave. However, these waves have now been modified by phase factors that account for the Coulomb interaction.

2.1.3. Derivation of the T-Matrix. Let H be the Hamiltonian of a particular system, and let the possible ways of splitting H be called arrangement channels. Then, for a given channel c,

$$H = H_c + V_c. \tag{39}$$

Let $\Phi_{c\gamma}$ be the eigenstates of H_c such that

$$H_c\Phi_{c\gamma} = E_{c\gamma}\Phi_{c\gamma}. \tag{40}$$

Here, γ contains all the information about the particles when they are in the asymptotic region of channel c. In scattering problems, it is typical to split the Hamiltonian into either the initial or final arrangement channel. For the initial channel,

$$H = H_i + V_i, \tag{41}$$

and for the final channel

$$H = H_f + V_f. \tag{42}$$

The corresponding eigenstates of H_i, denoted by $\Phi_{i\alpha}$, satisfy

$$H_i\Phi_{i\alpha} = E_i\Phi_{i\alpha}, \tag{43}$$

where the subscript α represents the initial state of the system in arrangement channel i. Similarly, the eigenstates $\Phi_{f\beta}$ of H_f, satisfy

$$H_f\Phi_{f\beta} = E_f\Phi_{f\beta}, \tag{44}$$

where β represents the final state of the system in arrangement channel f. To derive the T-Matrix, it is convenient to begin with a Hamiltonian that has only one arrangement channel,

$$H = H_0 + V, \tag{45}$$

where H_0 is the unperturbed Hamiltonian that governs the particles when they are far apart, and V is the interaction of the particles. Let the eigenstates of the full

Hamiltonian be Ψ_α with corresponding energies E_α, such that

$$H\Psi_\alpha = E_\alpha \Psi_\alpha. \tag{46}$$

Let the eigenstates of H_0 be denoted by $\Phi_\alpha, \Phi_\beta, \cdots$. These states are orthonormal,

$$\langle \Phi_\beta \mid \Phi_\alpha \rangle = \delta_{\alpha\beta}, \tag{47}$$

and form a complete set

$$\sum_\alpha \mid \Phi_\alpha \rangle \langle \Phi_\alpha \mid = 1. \tag{48}$$

For this Hamiltonian, there exists the unitary evolution operator $U(t, t')$ in the interaction picture given by

$$U(t, t') = e^{iH_0 t} e^{-iH(t-t')} e^{-iH_0 t'}. \tag{49}$$

The Møller operators, which convert an eigenstate governed by H_0 into an eigenstate of H at $t = 0$, are defined as

$$\Omega^{(\pm)} = U\left(0, \mp\infty\right) \tag{50}$$

and

$$\Omega^{(\pm)^\dagger} = U\left(\mp\infty, 0\right). \tag{51}$$

Then, the eigenstates of the full Hamiltonian can be expressed in terms of the eigenstates of the unperturbed Hamiltonian and the Møller operators as

$$\mid \Psi_\alpha^{(\pm)} \rangle = \Omega^{(\pm)} \mid \Phi_\alpha \rangle. \tag{52}$$

This implies that

$$\langle \Phi_\beta \mid \Omega^{\pm} \mid \Phi_\alpha \rangle = \langle \Phi_\beta \mid \Psi_\alpha \rangle. \tag{53}$$

Note that the Møller operators of equation (50) can now be rewritten as[5]

$$\Omega^{(\pm)} = \lim_{t \to \mp\infty} U(0,t) \tag{54}$$

$$= \lim_{t \to \mp\infty} e^{iHt} e^{-iH_0 t} \tag{55}$$

$$= \lim_{\varepsilon \to 0^+} \mp\varepsilon \int_0^{\mp\infty} e^{\pm\varepsilon t} e^{iHt} e^{-iH_0 t} dt. \tag{56}$$

Using the completeness relation of equation (48), the Møller operators can then be written as

$$\Omega^{(\pm)} = \lim_{\varepsilon \to 0^+} \mp\varepsilon \sum_\alpha \int_0^{\mp\infty} e^{\pm\varepsilon} e^{iHt} \mid \Phi_\alpha \rangle\langle \Phi_\alpha \mid e^{-iH_0 t} dt \tag{57}$$

$$= \lim_{\varepsilon \to 0^+} \mp\varepsilon \sum_\alpha \int_0^{\mp\infty} e^{\pm\varepsilon} e^{iHt} \mid \Phi_\alpha \rangle\langle \Phi_\alpha \mid e^{-iE_\alpha t} dt \tag{58}$$

$$= \lim_{\varepsilon \to 0^+} \mp\varepsilon \sum_\alpha \int_0^{\mp\infty} e^{i(H - E_\alpha \mp i\varepsilon)t} \mid \Phi_\alpha \rangle\langle \Phi_\alpha \mid dt \tag{59}$$

$$= \lim_{\varepsilon \to 0^+} \sum_\alpha \frac{\pm i\varepsilon}{E_\alpha - H \pm i\varepsilon} \mid \Phi_\alpha \rangle\langle \Phi_\alpha \mid . \tag{60}$$

Changing the summation index to α' and multiplying both sides by $\mid \Phi_\alpha \rangle$ gives

$$\Omega^{(\pm)} \mid \Phi_\alpha \rangle = \lim_{\varepsilon \to 0^+} \sum_{\alpha'} \frac{\pm i\varepsilon}{E_\alpha - H \pm i\varepsilon} \mid \Phi_\alpha \rangle \delta_{\alpha,\alpha'}, \tag{61}$$

and finally,

$$\mid \Psi_\alpha^{(\pm)} \rangle = \lim_{\varepsilon \to 0^+} \frac{\pm i\varepsilon}{E_\alpha - H \pm i\varepsilon} \mid \Phi_\alpha \rangle. \tag{62}$$

[5]The last step requires the limiting procedure [177], $\lim_{t \to -\infty} F(t) = \lim_{\varepsilon \to 0} \varepsilon \int_{-\infty}^{0} e^{\varepsilon t'} F(t') dt'$ and $\lim_{t \to \infty} F(t) = \lim_{\varepsilon \to 0} \varepsilon \int_0^{\infty} e^{-\varepsilon t'} F(t') dt'$.

It is now useful to note some relationships using the Møller operators. In general,

$$\Omega^{(\pm)^\dagger}\Omega^{(\pm)} = 1 = \sum_\alpha \mid \Phi_\alpha\rangle\langle\Phi_\alpha \mid \tag{63}$$

$$\Omega^{(\pm)}\Omega^{(\pm)^\dagger} = \sum_\alpha \mid \Psi_\alpha^{(\pm)}\rangle\langle\Psi_\alpha^{(\pm)} \mid \neq 1. \tag{64}$$

Note that the states $\mid \Psi_\alpha^{(\pm)}\rangle$ do not form a compete set because they do not include bound states. Letting $\mid \Psi^B\rangle$ denote a bound state leads to

$$\sum_\alpha \mid \Psi_\alpha^{(\pm)}\rangle\langle\Psi_\alpha^{(\pm)} \mid + \sum_B \mid \Psi^B\rangle\langle\Psi^B \mid = 1. \tag{65}$$

Therefore,

$$\Omega^{(\pm)}\Omega^{(\pm)^\dagger} = 1 - \sum_B \mid \Psi^B\rangle\langle\Psi^B \mid . \tag{66}$$

If the operator $\Lambda = \sum_B \mid \Psi^B\rangle\langle\Psi^B \mid$ is introduced as the projection operator onto bound states of H, then

$$\Omega^{(\pm)}\Omega^{(\pm)^\dagger} = 1 - \Lambda. \tag{67}$$

It can then be concluded that the Møller operators are only unitary if H and H_0 have no bound states. Also,

$$H\Omega^{(\pm)} = \Omega^{(\pm)}H_0 \tag{68}$$

$$\Omega^{(\pm)^\dagger}H = H_0\Omega^{(\pm)^\dagger} \tag{69}$$

$$\Omega^{(\pm)^\dagger}\Lambda = 0. \tag{70}$$

It is useful to generalize the Møller operators to the case where H can be split into several possible arrangement channels. Let

$$\Lambda_c = \sum_\gamma \mid \Phi_{c\gamma}\rangle\langle\Phi_{c\gamma} \mid \tag{71}$$

be the channel projection operator for channel c, where the sum over γ represents a sum over states within channel c. The Møller operators associated with channel c are defined as

$$\Omega_c^{(\pm)} = U_c\left(0, \mp\infty\right)\Lambda_c, \tag{72}$$

and

$$\Omega_c^{(\pm)^\dagger} = \Lambda_c U_c\left(\mp\infty, 0\right). \tag{73}$$

Then, the eigenstates of H at $t = 0$ are

$$\mid \Psi_{c\gamma}^{(\pm)}\rangle = \Omega_c^{(\pm)} \mid \Phi_{c\gamma}\rangle, \tag{74}$$

and specifically for the initial and final arrangement channels,

$$\mid \Psi_{i\alpha}^{(\pm)}\rangle = \Omega_i^{(\pm)} \mid \Phi_{i\alpha}\rangle \tag{75}$$

and

$$\mid \Psi_{f\beta}^{(\pm)}\rangle = \Omega_f^{(\pm)} \mid \Phi_{f\beta}\rangle. \tag{76}$$

By generalizing equations (49) through (70), in general

$$\Omega_c^{(\pm)^\dagger}\Omega_c^{(\pm)} = \Lambda_c. \tag{77}$$

However, unlike equation (47), in general for two different arrangement channels c and c',

$$\langle\Phi_{c\gamma}|\Phi_{c'\gamma'}\rangle \neq 0, \tag{78}$$

and specifically

$$\langle\Phi_{f\beta}|\Phi_{i\alpha}\rangle \neq 0. \tag{79}$$

This implies that the eigenstates of two different Hamiltonians, H_i and H_f, are not necessarily orthogonal.

However, it can be concluded that

$$\langle \Psi_b^{(\pm)} | \Psi_a^{(\pm)} \rangle = \delta_{ba} \tag{80}$$

since solutions of the full Hamiltonian are orthonormal. Further generalizations show that

$$\Lambda_c \Lambda_{c'} \neq 0 \tag{81}$$

$$\Omega_{c'}^{(\pm)^\dagger} \Omega_c^{(\pm)} = \Lambda_c \delta_{cc'} \tag{82}$$

$$\sum_c \Omega_c^{(\pm)} \Omega_c^{(\pm)^\dagger} = 1 - \Lambda \tag{83}$$

$$H \Omega_c^{(\pm)} = \Omega_c^{(\pm)} H_c \tag{84}$$

$$\Omega_{c'}^{(\pm)^\dagger} \Lambda = 0. \tag{85}$$

Then, in general,

$$\mid \Psi_{c\gamma}^{(\pm)} \rangle = \lim_{\varepsilon \to 0^+} \frac{\pm i\varepsilon}{E_{c\gamma} - H \pm i\varepsilon} \mid \Phi_{c\gamma} \rangle. \tag{86}$$

Recalling that $H_c \mid \Phi_{c\gamma} \rangle = E_{c\gamma} \mid \Phi_{c\gamma} \rangle$ and $H = H_c + V_c$, a little mathematical manipulation gives

$$\mid \Psi_{c\gamma}^{(\pm)} \rangle = \mid \Phi_{c\gamma} \rangle + \lim_{\varepsilon \to 0^+} \frac{V_c}{E_{c\gamma} - H \pm i\varepsilon} \mid \Phi_{c\gamma} \rangle. \tag{87}$$

Recall from potential scattering the form of the scattering amplitude (equation (21) or (33)) is

$$f(k,\theta,\varphi) = -\frac{\mu}{2\pi}\langle\Phi_{\vec{k}_f} \mid V \mid \psi^{(+)}_{\vec{k}_i}\rangle \tag{88}$$

$$= -\frac{\mu}{2\pi}\langle\Phi_{\vec{k}_f} \mid V\Omega^{(+)} \mid \Phi_{\vec{k}_i}\rangle. \tag{89}$$

Finally, the transition operator T can be defined as

$$T = V\Omega^{(\pm)}, \tag{90}$$

with matrix elements given by

$$T_{fi} = \langle\Phi_{\vec{k}_f} \mid V\Omega^{(\pm)} \mid \Phi_{\vec{k}_i}\rangle. \tag{91}$$

Now, rewriting equation (87) for the final channel gives

$$\mid \Psi^{(\pm)}_{\vec{k}_f}\rangle = \mid \Phi_{\vec{k}_f}\rangle + \lim_{\varepsilon\to 0^+} \frac{V_f}{E_f - H \pm i\varepsilon} \mid \Phi_{\vec{k}_f}\rangle. \tag{92}$$

Multiplying both sides by $\langle\Phi_{k_f} \mid$ gives

$$\Omega^{(\pm)}_f = 1 + \lim_{\varepsilon\to 0^+} \frac{1}{E_f - H \pm i\varepsilon} V_f. \tag{93}$$

Thus,

$$T = V_i + \lim_{\varepsilon\to 0^+} V_f \frac{1}{E_f - H \pm i\varepsilon} V_i. \tag{94}$$

Consider the matrix elements T_{fi}.

$$T_{fi} = \langle \Phi_{\vec{k}_f} \mid V_i \mid \Phi_{\vec{k}_i} \rangle + \langle \Phi_{\vec{k}_f} \mid V_f \frac{1}{E_f - H \pm i\varepsilon} V_i \mid \Phi_{\vec{k}_i} \rangle \tag{95}$$

$$= \langle \Phi_{\vec{k}_f} \mid \left(1 + V_f \frac{1}{E_f - H \pm i\varepsilon} \right) V_i \mid \Phi_{\vec{k}_i} \rangle \tag{96}$$

$$T_{fi} = \langle \Psi^{(-)}_{\vec{k}_f} \mid V_i \mid \Phi_{\vec{k}_i} \rangle \tag{97}$$

This is the prior form of the T-Matrix. Analogously, the post form can be written as

$$T_{fi} = \langle \Phi_{\vec{k}_f} \mid V_f \mid \Psi^{(+)}_{\vec{k}_i} \rangle. \tag{98}$$

Note that if the exact scattering wave functions are used, the post and prior forms of the T-Matrix are equivalent.

2.1.4. Two Potential Formulation. Recall from equations (97) and (98) that the T-matrix can be written in either the post or prior form as

$$T_{fi} = \langle \Psi^{(-)}_{\vec{k}_f} \mid V_i \mid \Phi_{\vec{k}_i} \rangle = \langle \Phi_{\vec{k}_f} \mid V_f \mid \Psi^{(+)}_{\vec{k}_i} \rangle. \tag{99}$$

In the two potential formulation, the initial or final potential (V_i or V_f) is written as the sum of two potentials such that

$$V_i = U_i + W_i \tag{100}$$

and

$$V_f = U_f + W_f. \tag{101}$$

Then,

$$T_{fi} = \langle \Psi^{(-)}_{\vec{k}_f} \mid U_i + W_i \mid \Phi_{\vec{k}_i} \rangle = \langle \Phi_{\vec{k}_f} \mid U_f + W_f \mid \Psi^{(+)}_{\vec{k}_i} \rangle. \tag{102}$$

Focusing on the post form, $\langle \Phi_{\vec{k}_f} \mid$ can be written in terms of distorted waves, $\langle \chi^{(-)}_{\vec{k}_f} \mid$.

$$\langle \Phi_{\vec{k}_f} \mid = \langle \chi^{(-)}_{\vec{k}_f} \mid - \langle \Phi_{\vec{k}_f} \mid U_f \frac{1}{E_f - \overline{H}_f + i\varepsilon}, \tag{103}$$

where $\overline{H}_f = H_f + U_f$. The distorted waves are continuum waves that have been distorted by the potential U_f, and are solutions of the Lippmann-Schwinger equation

$$\mid \chi^{(-)}_{\vec{k}_f} \rangle = \mid \Phi_{\vec{k}_f} \rangle + \frac{1}{E_f - \overline{H}_f - i\varepsilon} U_f \mid \Phi_{\vec{k}_f} \rangle. \tag{104}$$

Combining equations (102) and (103) gives the post form of the T-Matrix,

$$T^{post}_{fi} = \langle \chi^{(-)}_{\vec{k}_f} \mid U_f + W_f \mid \Psi^{(+)}_{\vec{k}_i} \rangle - \langle \Phi_{\vec{k}_f} \mid U_f \frac{1}{E_f - \overline{H}_f + i\varepsilon} (U_f + W_f) \mid \Psi^{(+)}_{\vec{k}_i} \rangle \tag{105}$$

$$= \langle \chi^{(-)}_{\vec{k}_f} \mid V_i - W_f \mid \Phi_{\vec{k}_i} \rangle + \langle \chi^{(-)}_{\vec{k}_f} \mid W_f \mid \Psi^{(+)}_{\vec{k}_i} \rangle. \tag{106}$$

Similarly the prior form of the T-Matrix is given by

$$T^{prior}_{fi} = \langle \Phi_{\vec{k}_f} \mid V_f - W_i \mid \chi^{(+)}_{\vec{k}_i} \rangle + \langle \Psi^{(-)}_{\vec{k}_f} \mid W_i \mid \chi^{(+)}_{\vec{k}_i} \rangle, \tag{107}$$

where $\mid \chi^{(+)}_{\vec{k}_i} \rangle$ are now distorted waves for the potential U_i. Note that if U_i or U_f can only cause elastic scattering, the first term in equations (106) and (107) is zero.

2.1.5. Differential Cross Sections. The differential cross section $d\sigma_{fi}/d\Omega_f$ can be related to the squared magnitude of the T-matrix through a multiplicative factor involving particle masses and momenta. This factor depends on the process being studied, and can be derived using Fermi's Golden Rule. For SC, TE, and DC, the factor is the same, and derived below.

Consider Fermi's Golden Rule for an incident projectile that is scattered from a target atom with energy E_f into a solid angle $d\Omega_f$. The transition rate is given by

$$d\omega_{fi} = 2\pi \mid T_{fi} \mid^2 \rho(E_f), \tag{108}$$

where $\rho(E_1)$ is the density of final states. Then,

$$d\sigma_{fi} = \frac{d\omega_{fi}}{\Phi}, \tag{109}$$

where Φ is the flux of the incident projectile. This can be written as the speed of the incident particle times the number density n, or number of particles per volume,

$$\Phi = v_i n. \tag{110}$$

The number density is simply given by

$$n = \mid \beta_i(\vec{r_1}) \mid^2, \tag{111}$$

where $\beta_i(\vec{r}_1)$ is the plane wave of equation (13). Then the flux becomes

$$\Phi = \frac{v_i}{(2\pi)^3}. \tag{112}$$

Combining equations (108) and (111) gives

$$d\sigma_{fi} = \frac{d\omega_{fi}(2\pi)^3}{v_i}. \tag{113}$$

The speed of the incident particle v_i can be written as

$$v_i = \frac{k_i}{\mu_{pa}}, \tag{114}$$

where μ_{pa} is the reduced mass of the projectile and target atom. Then,

$$d\sigma_{fi} = (2\pi)^4 \frac{\mu_{pa}}{k_i} \mid T_{fi} \mid^2 \rho(E_f), \tag{115}$$

and the density of final states is given by

$$\rho(E_f)dE_f = k_f^2 dk_f d\Omega_f. \tag{116}$$

The energy of the scattered projectile E_f can be written in terms of the momentum of the scattered projectile and the reduced mass,

$$E_f = \frac{k_f^2}{2\mu_{pi}}, \tag{117}$$

and therefore,

$$dE_f = \frac{k_f}{\mu_{pi}} dk_f. \tag{118}$$

Combining equations (116) and (118) gives

$$\rho(E_f) = \mu_{pi} k_f. \tag{119}$$

Then, the differential cross section for SC, TE, and DC becomes

$$\frac{d\sigma_{fi}}{d\Omega_f} = (2\pi)^4 \mu_{pa}\mu_{pi}\frac{k_f}{k_i} \mid T_{fi} \mid^2 . \tag{120}$$

A similar derivation for EI yields

$$\frac{d^5\sigma}{d\Omega_p d\Omega_e dE_e} = \mu_{pa}\mu_{ie}\frac{k_f k_e}{k_i} \mid T_{fi} \mid^2, \tag{121}$$

where $d\Omega_e$ is the solid angle into which the ejected electron is scattered, E_e is the energy of the ejected electron, and k_e is the wavevector of the ejected electron.

2.2. EXCITATION-IONIZATION

This section contains the theory for the models used in calculating FDCS for electron-impact excitation-ionization of helium. Results using the models presented here are shown in Section 3.1. For excitation-ionization, the FDCS as derived in section 2.1.5 is given by

$$\frac{d^5\sigma}{d\Omega_f d\Omega_e dE_e} = \mu_{pa}\mu_{ie}\frac{k_f k_e}{k_i} \mid T_{fi} \mid^2 \tag{122}$$

where μ_{pa} is the reduced mass of the projectile and the target atom, μ_{ie} is the reduced mass of the residual ion and electron, and $\vec{k}_i$ ($\vec{k}_f$) is the wavevector of the initial (scattered) projectile. It is differential in projectile solid angle, as well as ejected electron solid angle and energy.

2.2.1. 4-Body Distorted Wave (4DW) Model. The prior form of the T-Matrix (107) is evaluated for the 4DW model for electron-impact excitation-ionization of helium. Because the distorting potential U_i causes only elastic scattering in this case, the T-Matrix is given by

$$T_{fi} = \langle \Psi_f^{(-)} \mid W_i \mid \Psi_i \rangle = \langle \Psi_f^{(-)} \mid V_i - U_i \mid \Psi_i \rangle, \tag{123}$$

where

$$V_i = \frac{Z_p Z_{nuc}}{r_1} + \frac{Z_p Z_e}{r_{12}} + \frac{Z_p Z_e}{r_{13}} \tag{124}$$

is the initial state projectile-atom interaction. Here, Z_p, Z_{nuc}, and Z_e are the charges of the projectile, nucleus, and electron respectively, and r_1, r_{12}, and r_{13} are the

magnitudes of the relative coordinates for the projectile-target nucleus and projectile-target electrons (shown in figure 2.1).

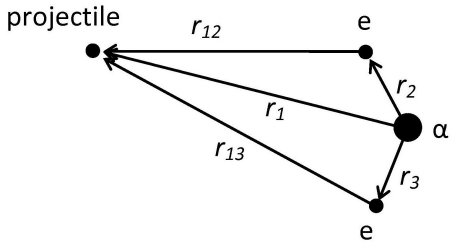

Figure 2.1. Coordinate system for the projectile-helium atom system, in which r_1, r_{12}, and r_{13} are the magnitudes of the relative coordinates of the projectile to the helium nucleus and atomic electrons respectively.

The initial state wave function Ψ_i is given by

$$\Psi_i = \chi_i(\vec{r}_1)\xi\left(\vec{r}_2, \vec{r}_3\right). \tag{125}$$

Here, $\chi_i(\vec{r}_1)$ is a distorted wave for the incident projectile, which is a solution of the Schrödinger equation for the distorting potential U_i. This distorting potential is a spherically symmetric approximation to V_i. Therefore, the term $V_i - U_i$ in (123) represents the nonspherical part of the initial state projectile-atom interaction. The term $\xi\left(\vec{r}_2, \vec{r}_3\right)$ is the ground state wave function for helium, which is given by a 20 term Hylleraas [176] wave function that includes both radial and angular correlations.

The final-state wave function $\Psi_f^{(-)}$ is approximated by

$$\Psi_f^{(-)} = \chi_f(\vec{r}_1)\chi_e\left(\vec{r}_2\right)\varphi_{nlm}\left(\vec{r}_3\right)C(\gamma, \vec{k}_{12}, \vec{r}_{12}), \tag{126}$$

where for clarity electron 2 is labeled as the "slow" ejected electron and electron 3 as the remaining bound electron of the He^+ ion. The two continuum distorted waves $\chi_f(\vec{r}_1)$ and $\chi_e(\vec{r}_2)$ are solutions of the Schrödinger equation for the final state distorting potential U_f, which is a spherically symmetric approximation for the potential of the He^+ ion. The term $\varphi_{nlm}(\vec{r}_3)$ is the hydrogenic wave function for the He^+ ion, and $C(\gamma, \vec{k}_{12}, \vec{r}_{12})$ is the Coulomb distortion factor that accounts for the electron-electron interaction between the two continuum electrons in the final state. This term is often referred to as the "C-factor" or post collision interaction (PCI). It is exact, and is given by

$$C(\gamma, \vec{k}_{12}, \vec{r}_{12}) = e^{-\pi\gamma/2}\Gamma(1+i\gamma)_1F_1(-i\gamma, 1, i(k_{12}r_{12} + \vec{k}_{12}\cdot\vec{r}_{12})), \tag{127}$$

where ${}_1F_1$ is a confluent hypergeometric function and $\Gamma(1+i\gamma)$ is the gamma function. Here, $\gamma = \mu_{pe}Z_pZ_e/k_{12}$, where μ_{pe} is the reduced mass of the projectile and the ejected electron and $\vec{k}_{12}$ is the relative momentum between the two outgoing electrons.

Because electrons are indistinguishable, it is necessary to make the final state spatial wave function symmetric with respect to the two atomic electron coordinates. Thus, for the 4DW calculations presented in section 3.1, the final state wave function that is used is of the form

$$\Psi_f^{sym} = \chi_f(\vec{r}_1)\left[\chi_e(\vec{r}_2)\varphi_{nlm}(\vec{r}_3)C(\gamma, \vec{k}_{12}, \vec{r}_{12}) + \chi_e(\vec{r}_3)\varphi_{nlm}(\vec{r}_2)C(\gamma, \vec{k}_{13}, \vec{r}_{13})\right]. \tag{128}$$

In the 4DW T-matrix of equation (123), the interactions that are contained to first order in perturbation theory are those in $V_i - U_i$ (i.e. the nonspherical part of the initial state projectile-atom interaction). Since any interaction contained in the final state wave function is contained to all orders of perturbation theory, the inclusion of the final state electron-electron Coulomb interaction in the wave function ensures that PCI is included to all orders of perturbation theory. When one solves

the Schrödinger equation for a distorting potential U, the physical effect contained in the resulting wave function is elastic scattering from the spherically symmetric atom (ion) represented by U. Consequently, using the He^+ distorting potential U_f to calculate the two final state continuum-electron wave functions guarantees that elastic scattering of the continuum-electrons from the spherically symmetric distorting potential U_f representing the ion is also contained to all orders of perturbation theory. Similarly, the initial state distorted wave contains elastic scattering from the spherically symmetric initial-state distorting potential U_i to all orders of perturbation theory.

It is also important to note that the final state wave function (126) is an asymptotically exact solution to the Schrödinger equation [178, 179]. For the three-body problem, it has been shown that 'asymptotic' means for one particle to be greater than about $2a_0$ from the other two, which can be arbitrarily close to each other [180]. As a result, one would expect that the wave function (126) is also accurate for relatively small separations of the four particles.

It has been observed for single ionization that orthogonalizing the ejected electron wave function to the initial bound state wave function using Gram-Schmidt orthogonalization normally improves agreement with experiment, although it is not required by the theory [181]. Because simultaneous excitation-ionization involves two active electrons, it is necessary to generalize the orthogonalization procedure so that the final state wave function for the two active electrons $\chi_e(\vec{r}_2)\varphi_{nlm}(\vec{r}_3)$ is made orthogonal to the initial state wave function for the two bound state electrons $\xi(\vec{r}_2, \vec{r}_3)$. The four-body analogue to the three-body orthogonalization procedure gives the following form for the final state orthogonalized wave function, which is used in the results presented in Section 3.1:

$$\Psi_f^{orth}(\vec{r}_2, \vec{r}_3) = \chi_e(\vec{r}_2)\varphi_{nlm}(\vec{r}_3) - \xi(\vec{r}_2, \vec{r}_3) \int \chi_e(\vec{r}_2{}')\varphi_{nlm}(\vec{r}_3{}')\xi(\vec{r}_2{}', \vec{r}_3{}')d\vec{r}_2{}'d\vec{r}_3{}'. \quad (129)$$

2.2.2. First Born Approximation (FBA) Model. In addition to the 4DW model, an analogous calculation, which ignores all projectile-target interactions while treating the two atomic electrons exactly the same, is presented in Section 3.1. This approach is known as the first Born approximation (FBA) since the projectile wave functions are now plane waves. The FBA T-Matrix is given by

$$T_{fi} = \langle \Psi_f^{(-)} \mid V_i \mid \Psi_i \rangle \tag{130}$$

since the incident projectile wave function is a plane wave, and consequently $U_i = 0$.

The initial state projectile-atom interaction V_i is the same as in equation (124), and the initial and final state wave functions are given by

$$\Psi_i = \beta_i \left(\vec{r}_1\right) \xi \left(\vec{r}_2, \vec{r}_3\right) \tag{131}$$

and

$$\Psi_f = \beta_f \left(\vec{r}_1\right) \chi_e \left(\vec{r}_2\right) \varphi_{nlm} \left(\vec{r}_3\right), \tag{132}$$

where $\beta_{i,f} \left(\vec{r}_1\right)$ is a plane wave for the initial (final) state projectile given by equation (13). The helium atom wave function $\xi \left(\vec{r}_2, \vec{r}_3\right)$ is again a 20 term Hylleraas [176] wave function, $\chi_e \left(\vec{r}_2\right)$ is the distorted wave for the ejected electron calculated using the potential U_f, and $\varphi_{nlm} \left(\vec{r}_3\right)$ is the hydrogenic wave function for the residual He^+ ion. Note that the FBA model does not include PCI in the final state wave function, while the 4DW model does. Results of the FBA model are presented in Section 3.1.

2.3. SINGLE CHARGE TRANSFER AND TRANSFER-EXCITATION

This section contains the theoretical model used in the calculation of FDCS for SC and TE, the results of which are presented in Sections 3.2 and 3.3. The FDCS for SC and TE is differential only in scattering angle, and as derived in Section 2.1.5,

can be written as

$$\frac{d\sigma}{d\Omega} = (2\pi)^4 \mu_{pa}\mu_{pi}\frac{k_f}{k_i} \mid T_{fi} \mid^2, \tag{133}$$

where μ_{pa} is the reduced mass of the projectile and target atom, μ_{pi} is the reduced mass of the projectile and residual ion, and $\vec{k}_i$ ($\vec{k}_f$) is the wavevector of the incident (scattered) projectile.

2.3.1. 4-Body Transfer-Excitation (4BTE) Model. Similar to the 4DW model, the 4BTE model uses the prior form of the transition matrix T_{fi}, which is given by equation (123)

$$T_{fi} = \langle \Psi_f^{(-)} \mid W_i \mid \Psi_i \rangle. \tag{134}$$

The initial state wave function is given by

$$\Psi_i = \chi_p^i(\vec{R}_i)\xi_{He}(\vec{r}_2, \vec{r}_3), \tag{135}$$

where $\chi_p^i(\vec{R}_i)$ is the incident projectile wave function and $\xi_{He}(\vec{r}_2, \vec{r}_3)$ is the ground-state helium atom wave function. The final state wave function is given by

$$\Psi_f^{(-)} = \chi_p^f(\vec{R}_f)\phi_H(\vec{r}_{12})\psi_{He^+}(\vec{r}_3), \tag{136}$$

where $\chi_p^f(\vec{R}_f)$ is the scattered hydrogen wave function, $\psi_{_{He^+}}(\vec{r}_3)$ is the final state He^+ wave function, and $\phi_H(\vec{r}_{12})$ is the outgoing hydrogen wave function. Both $\phi_H(\vec{r}_{12})$ and $\psi_{He^+}(\vec{r}_3)$ are simply hydrogenic wave functions, and thus known exactly. For an incident plane wave, W_i is simply the projectile-target interaction potential V_i, given by equation (124)

$$V_i = \frac{Z_p Z_{nuc}}{r_1} + \frac{Z_p Z_e}{r_{12}} + \frac{Z_p Z_e}{r_{13}}. \tag{137}$$

Again, the final state wave function has been properly symmetrized in the calculations, but the electrons have been labeled here for clarity.

The calculations are performed in the center of mass frame, using the Jacobi coodinates [182] shown in figures 2.2 and 2.3. In this coordinate system, $\vec{R}_i$ is the

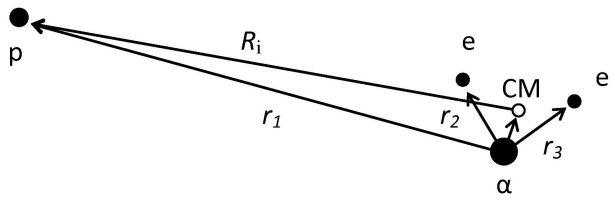

Figure 2.2. Jacobi coordinate system for the projectile-helium atom system.

relative vector between the projectile and the center of mass of the helium atom, and $\vec{R}_f$ is the relative vector between the center of mass of the hydrogen atom and the center of mass of the He^+ ion. They are given by

$$\vec{R}_i = \vec{r}_1 - \frac{m_e}{m_\alpha + 2m_e}(\vec{r}_2 + \vec{r}_3) \tag{138}$$

and

$$\vec{R}_f = \frac{m_e\vec{r}_2 + m_p\vec{r}_1}{m_p + m_e} - \frac{m_e}{m_e + m_\alpha}\vec{r}_3, \tag{139}$$

where m_e, m_α, and m_p are the masses of the electron, alpha particle, and projectile respectively. In the calculations presented in Section 3.3, two different wave functions for the incident projectile, ground-state helium atom, and scattered projectile are examined.

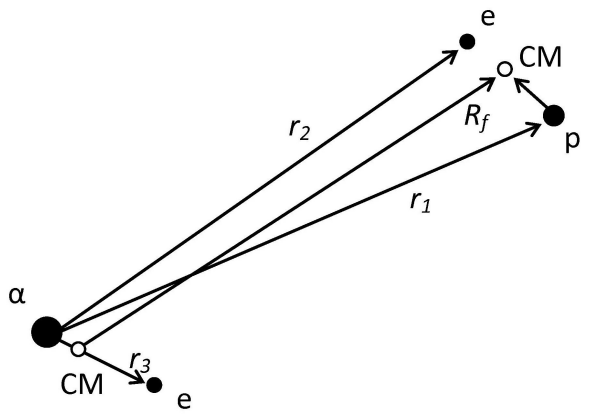

Figure 2.3. Jacobi coordinate system for the hydrogen-helium ion system.

For the incident projectile wave function, either a plane wave given by

$$\chi_p^i(\vec{R}_i) = \frac{e^{i\vec{k}_i\cdot\vec{R}_i}}{(2\pi)^{3/2}} \tag{140}$$

or an Eikonal[6] wave function [183] given by

$$\chi_p^i(\vec{R}_i) = \frac{e^{i\vec{k}_i\cdot\vec{R}_i}}{(2\pi)^{3/2}} \exp\left[i\frac{Z_p}{v_p}\ln\left(\frac{(v_p r_1 - \vec{v}_p\cdot\vec{r}_1)^{Z_{nuc}}}{(v_p r_{12} - \vec{v}_p\cdot\vec{r}_{12})(v_p r_{13} - \vec{v}_p\cdot\vec{r}_{13})}\right)\right] \tag{141}$$

is used, where $\vec{v}_p$ is the velocity of the incident projectile.

For the ground-state helium atom, either an analytic Hartree-Fock [184] wave function or a 20-term Hylleraas [176] wave function is used. Again, the Hartree-Fock wave function has no electron-electron correlation, while the Hylleraas wave function contains both radial and angular correlation.

[6]For the Eikonal calculation, the post form of the T-matrix was evaluated. See Appendix C for details.

For the scattered projectile, either a plane wave given by

$$\chi_p^f(\vec{R}_f) = \frac{e^{i\vec{k}_f\cdot\vec{R}_f}}{(2\pi)^{3/2}} \tag{142}$$

or a Coulomb wave given by

$$\chi_p^f(\vec{R}_f) = \frac{e^{i\vec{k}_f\cdot\vec{R}_f}}{(2\pi)^{3/2}} e^{-\pi\gamma/2}\Gamma(1+i\gamma)_1F_1(-i\gamma,1;i(k_fR_f+\vec{k}_f\cdot\vec{R}_f)) \tag{143}$$

is used, where $\gamma = \frac{Z_pZ_{He^+}}{v_H}$. The quantities Z_p and Z_{He^+} are the electric charges of the projectile and He^+ ion; v_H is the speed of the hydrogen atom. The FDCS for single charge transfer without excitation can also be evaluated using the 4BTE model by simply allowing the He^+ ion to be left in the ground state. Results of the 4BTE model for SC and TE are presented in Sections 3.2 and 3.3 respectively.

2.4. DOUBLE CHARGE TRANSFER

This section contains the theoretical model used in the calculation of FDCS for DC, and the corresponding results are presented in Section 3.4.

2.4.1. 4-Body Double Capture (4BDC) Model. The theory for DC is quite similar to that of SC or TE. Because the fully differential cross section for DC is again differential only in scattering angle, it is given by equation (133), and the corresponding T-Matrix is given by equation (123). The initial state wave function is the same as that of TE and equation (135). However, the final state wave function is now given by

$$\Psi_f^{(-)} = \chi_p^f(\vec{R}_f)\psi_{H^-}(\vec{r}_{12},\vec{r}_{13}), \tag{144}$$

where $\psi_{H^-}(\vec{r}_{12},\vec{r}_{13})$ is the wave function for the outgoing H^- ion, and $\chi_p^f(\vec{R}_f)$ is the scattered projectile wave function. The calculation is again performed in the center of mass frame, and the Jacobi coordinate $\vec{R}_f$ is now the relative vector between the alpha

particle and the center of mass of the H^- ion. Unlike SC or TE, it is now possible to examine the effects of correlation in both the initial and final bound state wave functions. Thus, in the calculations presented in Section 3.4, either a Variational wave function [185] or 20 parameter Hylleraas [176] wave function is used for the helium atom and H^- ion. The initial projectile is treated as a plane wave, and the final projectile is treated as a Coulomb wave, where $\gamma = \frac{Z_{H^-} Z_{He^{++}}}{v_{H^-}}$, with Z_{H^-} and $Z_{He^{++}}$ being the charges of the H^- and He^{++} ions, and v_{H^-} being the speed of the H^- ion.

3. RESULTS

3.1. EXCITATION-IONIZATION

Recall from Section 1.1 the process of EI, in which an incident electron collides with a helium atom, causing one of the atomic electrons to be ionized and the other to be promoted to an excited state of the ion. Results from the 4DW and FBA models of Sections 2.2.1 and 2.2.2 are compared to two different sets of experimental results, which involve excitation and ionization of the He^+ ion to either the $2p$ state or to the n = 2 or n = 3 states. In both cases, the individual angular momenta are not determined, and the FDCS contributions from the individual magnetic substates must be summed to allow for direct comparison with experiment.

3.1.1. Cross Normalized Results. FDCS for EI are presented in this section for a given incident projectile energy E_0, scattering angle θ_a, and ejected electron energy E_2 as a function of the ejected electron angle θ_e. The results in this section are presented for an incident projectile energy of 500 eV and two ejected electron energies of 3 eV and 10 eV. For each ejected electron energy, two different scattering angles of approximately 4° and 29° are shown. The experimental results are not absolute, and therefore must be normalized to one of the theories. However, the cross normalization between measurements is fixed, so only one normalization can be used for all four data sets. The experiment has been normalized to the 4DW model at the binary peak for $E_2 = 3$ eV and $\theta_a = 4.1°$, which is the largest cross section. Figure 3.1 shows both the 4DW and FBA calculations for excitation-ionization of helium with the ion left in the 2p state as a function of ejected electron angle θ_e [14]. The calculations are compared to the experimental results of Sakhelashvili et al. [10] and a second Born R-Matrix with pseudostates calculation (DWB2-RMPS) by Bartschat [10]. The DWB2-RMPS calculation has been divided by 1.8 to normalize it to the same point and provide the same shape comparison as in reference [10].

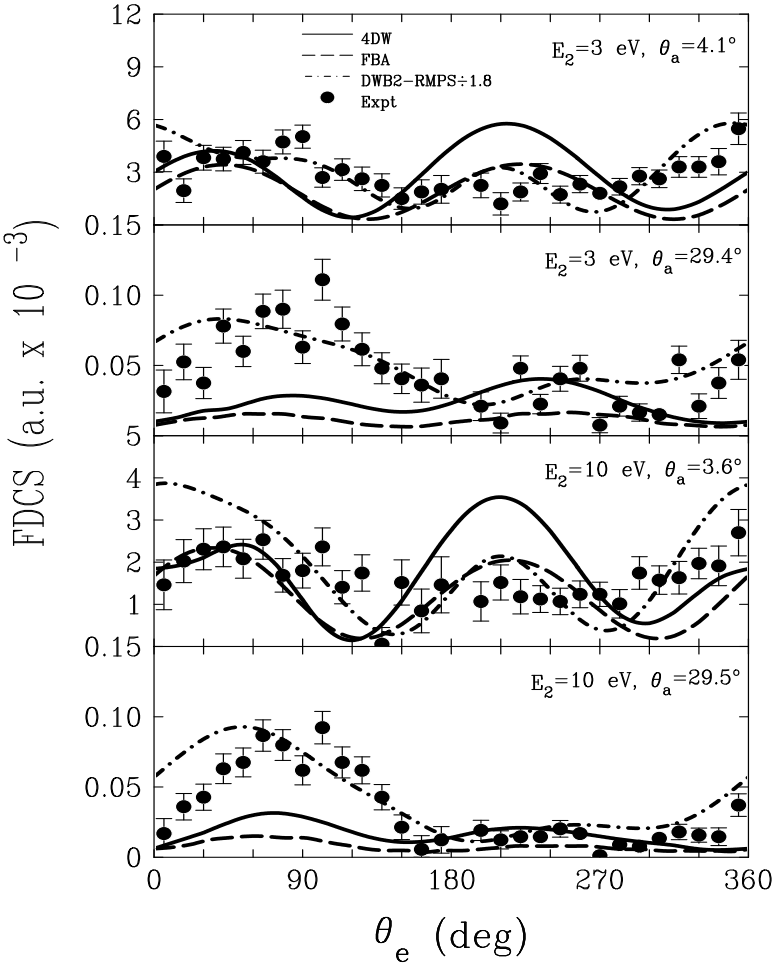

Figure 3.1. Theoretical FDCS for electron-impact excitation-ionization of helium as a function of ejected electron angle θ_e. Results of the 4DW, FBA, and DWB2-RMPS (divided by 1.8) models are compared to the relative experimental results of [10]. The incident energy is 500 eV. Experimental results have been normalized to the binary peak of the 4DW calculation at $E_2 = 3$ eV and $\theta_a = 4.1°$

A comparison of the 4DW and the FBA calculations reveals what effect the treatment of the projectile has on the FDCS. Figure 3.1 shows that the 4DW calculation predicts a larger recoil peak (peak near 220°) than the FBA, which is shifted slightly to smaller ejected electron angles. The 4DW also predicts a larger binary peak, which, in all but one case, has been shifted to larger ejected electron angles.

The observed angular shifts are exactly what one would expect from the final state PCI repulsion between the two continuum electrons.

In comparison with experiment, the 4DW does a reasonably good job of predicting the binary peaks for the small projectile scattering angles, but drastically underestimates the binary peak for large projectile scattering angles. Also, the 4DW overestimates the recoil peak for small scattering angles, while there is at least qualitative agreement for the recoil peak at large scattering angles.

Overall, the DWB2-RMPS results are in better agreement with the shape of the experimental data than the 4DW. The two theories differ in the treatment of the initial state interactions, ejected-electron-ion interaction, and PCI. The differences are: (1) the 4DW treats initial state interactions to first order and the DWB2-RMPS treats initial state interactions to second order; (2) the 4DW treats the ejected electron as a distorted wave, while the DWB2-RMPS treats the ejected electron as a close coupling wave function; and (3) the 4DW treats PCI to all orders of perturbation theory, while the DWB2-RMPS ignores PCI. Clearly, the shape of the FDCS is more sensitive to either initial state interactions or ejected-electron-ion interactions than to a proper treatment of PCI, at least for these kinematics. However, many of these conclusions could be affected by the choice of the normalization factor, and agreement with experiment could change drastically if one chose to normalize to something other than the largest cross sections. Thus, it is useful to study absolute experimental results.

3.1.2. Absolute Ratio Results. In this section, results are presented for ratios of the FDCS of leaving the ion in the n = 1 state divided by the FDCS of leaving the ion in the n = 2 (n = 3) state. Two different energy sharing cases are shown. In the case of symmetric energy sharing, the scattered electron and the ejected electron have the same energy. For asymmetric energy sharing, the two electrons have different energies. Figure 3.2 shows the experimental FDCS ratios of Bellm et al. [7,8]

along with the 4DW, FBA, and DWB2-RMPS calculations [14]. The top half of the figure shows results for asymmetric energy sharing with a scattered projectile energy of $E_1 = 200$ eV and an ejected electron energy of $E_2 = 44$ eV. The bottom half of the figure shows symmetric energy sharing with both final state continuum electrons having the same energy, i.e. $E_1 = E_2 = 44$ eV.

The first column in figure 3.2 shows the FDCS for ionization without excitation divided by the FDCS for ionization with excitation to the n = 2 state. Similarly, the second column shows the FDCS for leaving ion in the n = 1 state divided by the FDCS for leaving the ion in the n = 3 state. For the asymmetric energy sharing, the FBA model has been divided by 5, and the 4DW model has been divided by 3. For the symmetric energy sharing, the FBA has been divided by 5, while the 4DW has only been divided by 2. The DWB2-RMPS model, however, has no normalization factors. None of the calculations are in excellent agreement with experiment, but the 4DW provides probably the best agreement with the shape of the experimental data, while the DWB2-RMPS clearly has the best magnitude agreement.

Figure 3.3 shows the experimental results of Bellm et al. [186] and the 4DW, FBA, and DWB2-RMPS calculations [186]. The first column in this figure also shows the FDCS for ionization without excitation divided by the FDCS for ionization with excitation to the n = 2 state, and the second column shows the FDCS for leaving the ion in the n = 1 state divided by the FDCS for leaving the ion in the n = 3 state. These results are for asymmetric energy with a scattered projectile energy of 150 eV and an ejected electron energy of 20 eV.

A comparison of the 4DW and FBA models shows that for both asymmetric and symmetric energy sharing, a more accurate treatment of the projectile significantly improves both the shape and magnitude of the FDCS. However, the 4DW still overestimates the absolute magnitude of the experiment for the energies shown in figures 3.2 and 3.3. One possible reason for this disagreement in magnitude is the large

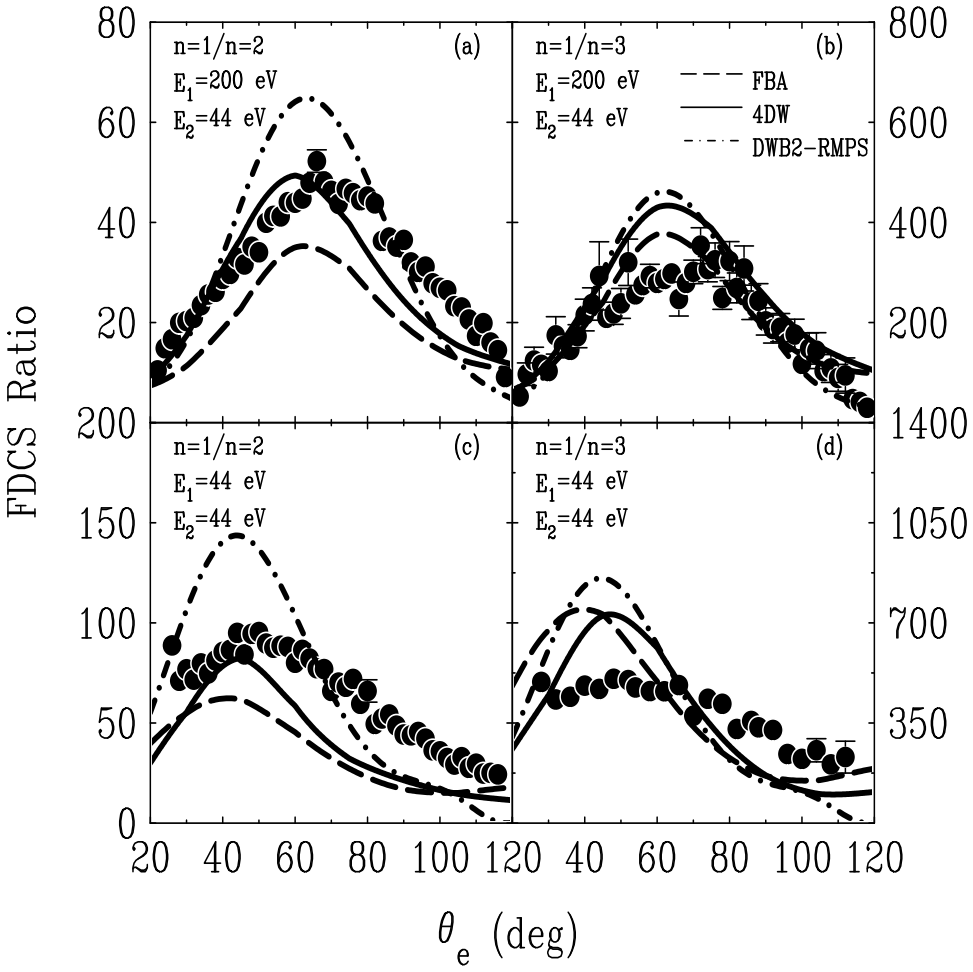

Figure 3.2. Theoretical results of the 4DW and FBA theories for FDCS ratios for excitation-ionization as a function of ejected electron angle θ_e with a scattering angle of $\theta_a = 32°$. The calculations are compared to a DWB2-RMPS calculation and absolute experimental data [8]. Incident projectile energies are: (a) E_0 = 268.6 eV (n = 1) and E_0 = 309.4 eV (n = 2); (b) E_0 = 268.6 eV (n = 1) and E_0 = 316.9 eV (n = 3); (c) E_0 = 112.6 eV (n = 1) and E_0 = 153.4 eV (n = 2); (d) E_0 = 112.6 eV (n = 1) and E_0 = 161.0 eV (n = 3). For (a) and (b), the FBA has been divided by 5, and the 4DW has been divided by 3. For (c) and (d), the FBA has been divided by 5, and the 4DW has been divided by 2.

projectile scattering angles. It has been seen in previous work with the Three-Body Distorted Wave model that the theory agreed nicely with the shape and magnitude of absolute experimental data for small projectile scattering angles. However, as the

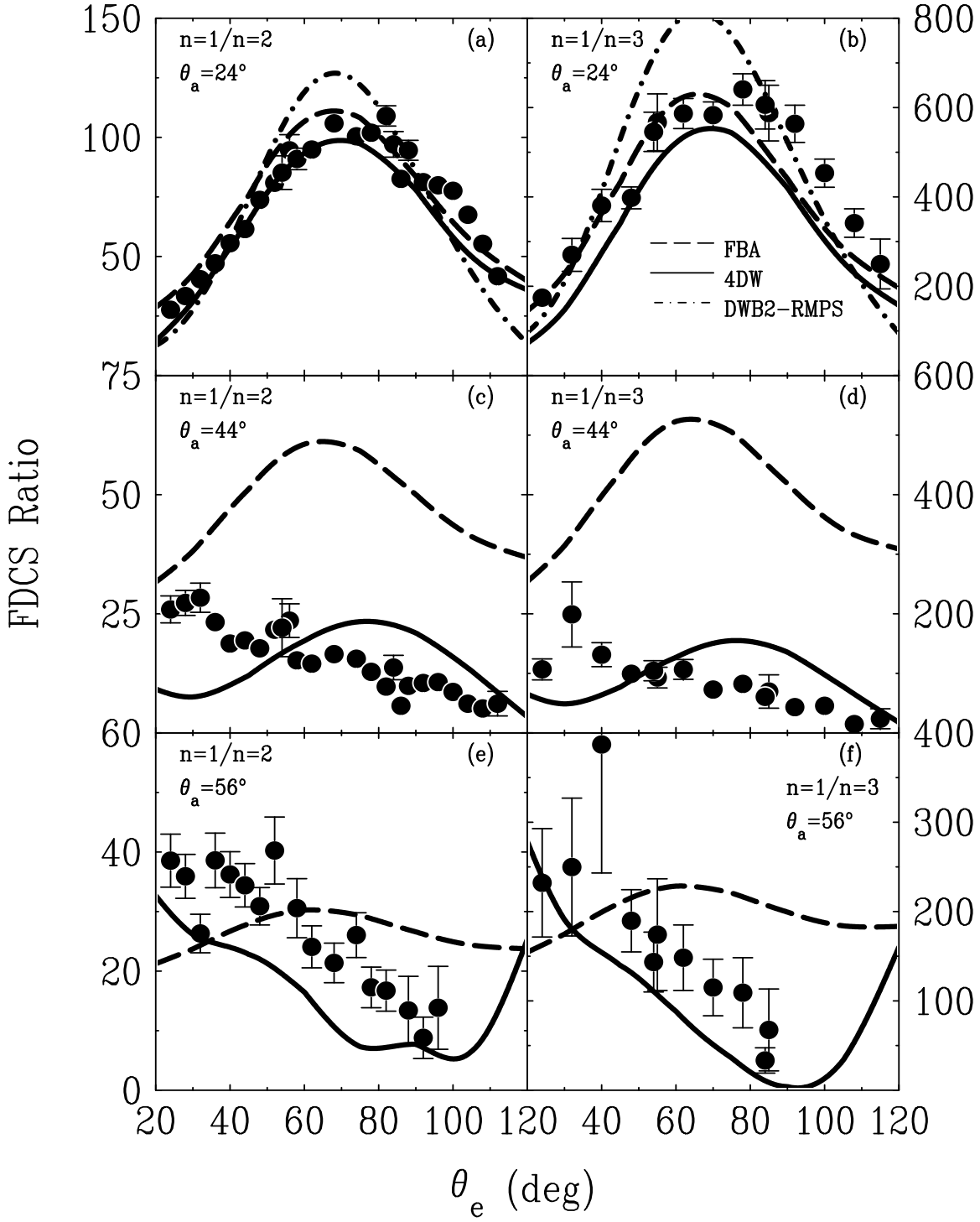

Figure 3.3. Theoretical results of the 4DW and FBA models for FDCS ratios for excitation-ionization as a function of ejected electron angle θ_e for a scattered projectile energy of 150 eV and an ionized electron energy of 20 eV. The calculations are again compared to a DWB2-RMPS calculation and absolute experimental data [8]. For panel (a), the 4DW and FBA have been divided by 2.5. For panel (b) the 4DW and FBA have been divided by 5, and the DWB2-RMPS has been divided by 2. All other calculations are absolute.

scattering angle increased, shape agreement remained, but the magnitude became incorrect [187]. Since the projectile scattering angles here are fairly large, it appears that a similar behavior is being observed. Dramatic shape differences between the 4DW and FBA can be seen in figure 3.3, particularly at 44° and 56°, while in figure 3.2, the FBA and 4DW exhibit similar shapes. For these two sets of energies, the relative speeds of the scattered and ejected electron is approximately the same. Thus, the effect of PCI in both cases should be approximately the same, and the resulting differences between the FBA and 4DW in both cases are most likely due to the distorted wave treatment of the projectile. This indicates that a distorted wave treatment is much more important at lower energies and larger scattering angles, as expected.

It is also interesting to note that, contrary to the results of figure 3.1, the 4DW agrees with the shape of the experimental data somewhat better than the DWB2-RMPS. Since the ejected electron energies are significantly higher in these cases, there should be much less difference between a close-coupling wave function and a distorted wave. This would suggest that the better shape agreement seen in figures 3.2 and 3.3 for the 4DW is a result of the better treatment of PCI in the 4DW. Also, the better shape agreement for the DWB2-RMPS seen in figure 3.1 for lower ejected-electron energies probably is a result of the better treatment of the ejected electron wave function in the DWB2-RMPS.

In all cases, the FBA overestimates the magnitude of experiment and only predicts the correct shape for asymmetric energy with the two smallest scattering angles. For asymmetric energy, the overestimation of the magnitude of the FBA is most likely due to the PW treatment of the projectile, and not the lack of PCI.

3.1.3. Absolute Results. "Absolute experimental" results for excitation-ionization with the He^+ ion left in the n = 2 (n = 3) state can be produced using the FDCS ratios of Section 3.1.2 by assuming that convergent close-coupling calculations

(CCC) for ionization without excitation are accurate, and using these to put the n = 2 (n = 3) data on an absolute scale [188]. Figures 3.4 and 3.5 show the theoretical results of the 4DW, FBA, DWB2-RMPS, and CCC models for ionization without excitation, and in figure 3.5 the experimental results of [8] are also included. As expected, the 4DW is significantly closer to the CCC than the FBA. However, the 4DW still overestimates the CCC, except for the largest scattering angles in figure 3.5, where both the shape and the magnitude differ greatly from the CCC.

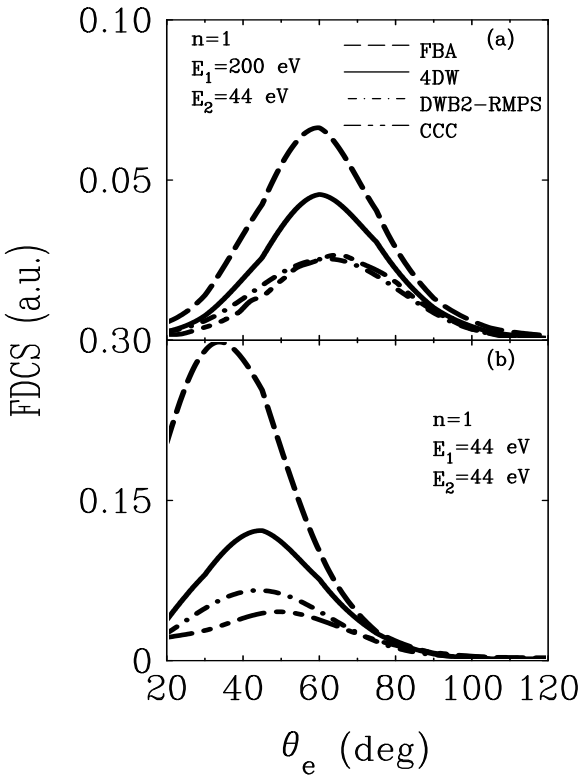

Figure 3.4. Comparison of theoretical calculations for ionization without excitation as a function of ejected electron angle θ_e with a scattering angle of $\theta_a = 32°$. The incident energies are (a) $E_0 = 268.6$ eV and (b) $E_0 = 112.6$ eV.

Figures 3.6 and 3.7 show FDCS for transitions leading to the He^+(n = 2) and He^+(n = 3) states. For asymmetric energy, it can be seen that the 4DW approach gives

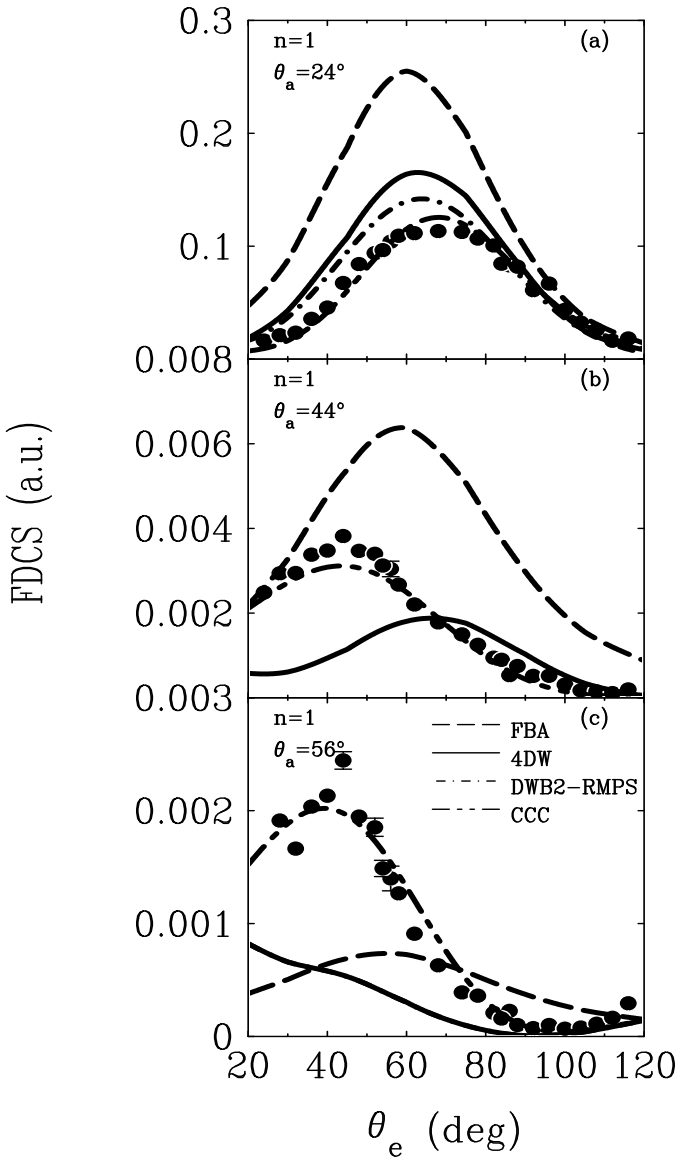

Figure 3.5. Comparison of theoretical calculations for ionization without excitation as a function of ejected electron angle θ_e with an incident energy of $E_0 = 194.6$ eV and an ejected electron energy of $E_2 = 20$ eV.

the best agreement with the shape of the "absolute experimental" data. However, the 4DW and FBA results shown in figures 3.6 and 3.7 have been multiplied by 2 and 2.5 for the n = 2 and n = 3 asymmetric energy sharing, respectively. This is to be contrasted with the symmetric energy sharing case, where the shape is not

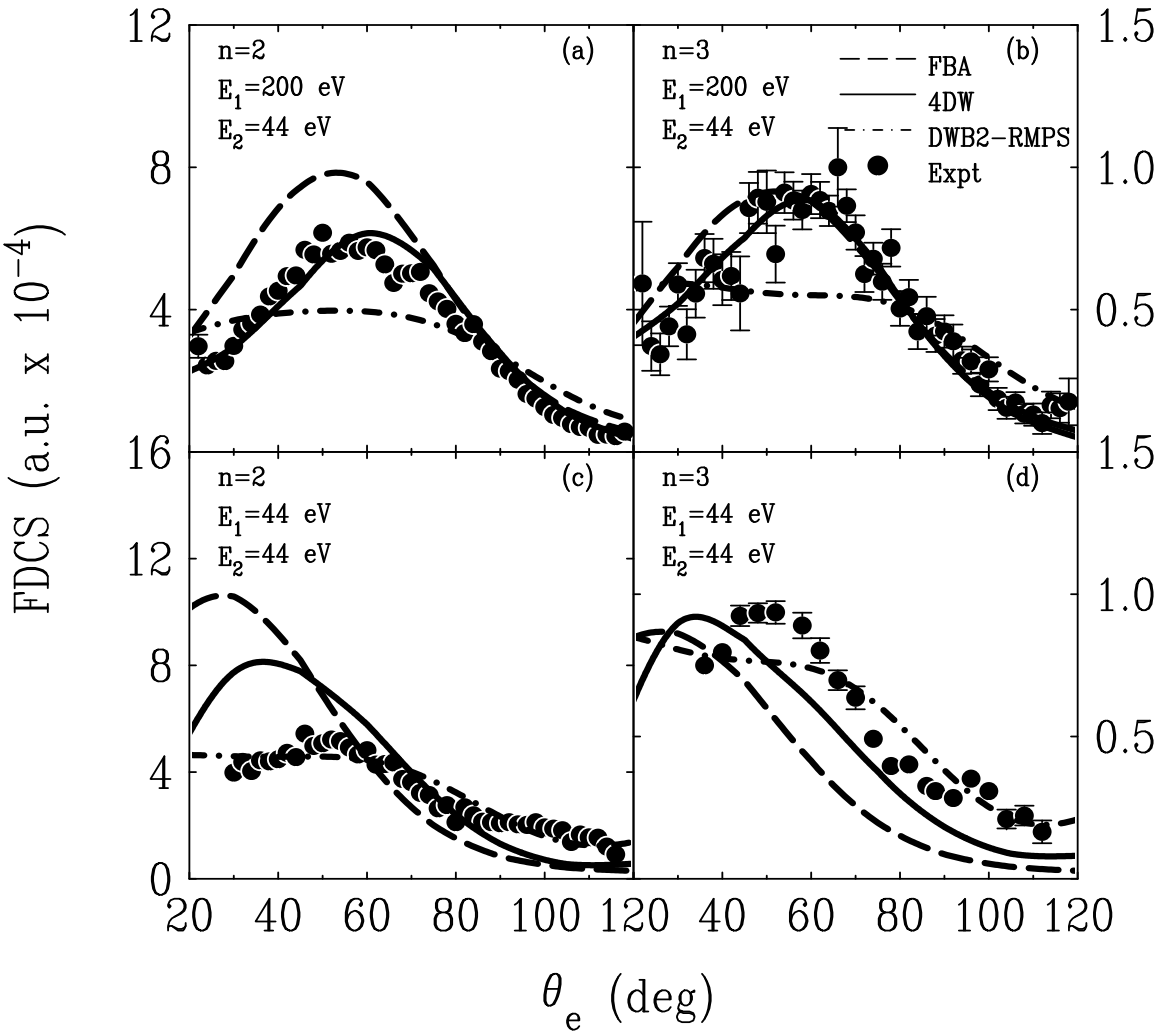

Figure 3.6. Absolute FDCS as a function of ejected electron angle θ_e with a scattering angle of $\theta_a = 32°$. The 4DW and FBA theories are compared to the DWB2-RMPS model and "absolute experimental" results [8]. The FBA and 4DW calculations have been multiplied by 2 and 2.5 in (a) and (b) respectively. Incident energies are the same as those listed for figure 3.2.

quite as good, but the magnitude is much closer to experiment since there are no normalization factors for this case. Particularly for the asymmetric energy case, the 4DW does better than the FBA and DWB2-RMPS in predicting both the shape and angular location for the binary peak. As mentioned above, this is likely due to the better treatment of PCI in the 4DW.

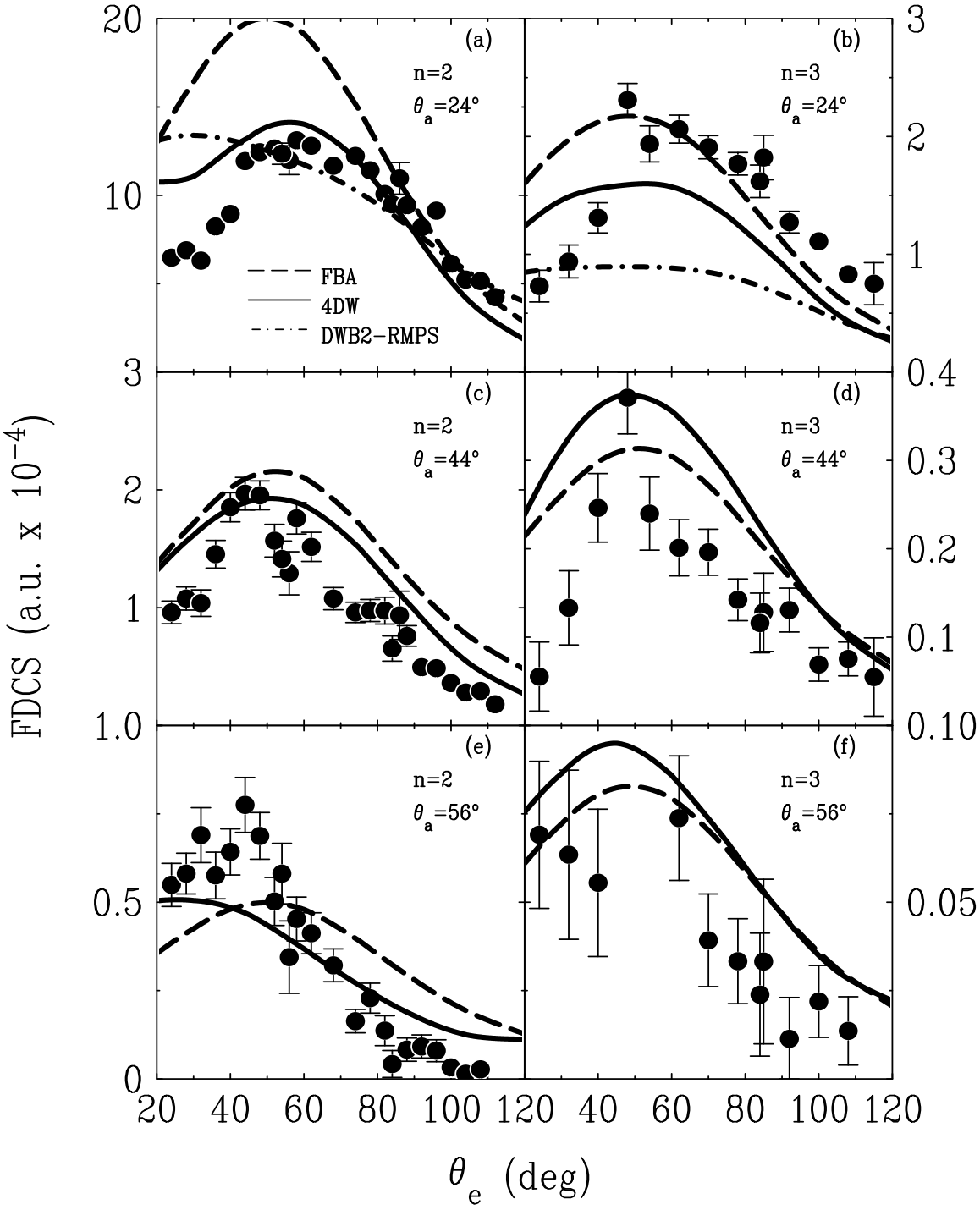

Figure 3.7. Absolute FDCS as a function of ejected electron angle θ_e with a scattered projectile energy of 150 eV and an ejected electron energy of 20 eV. The 4DW and FBA theories are compared to the DWB2-RMPS model and "absolute experimental" results [186]. The FBA and 4DW calculations have been multiplied by 2 for the n = 2 results and by 2.5 for the n = 3 results.

By examining figures 3.4 - 3.7 the source of the magnitude discrepancies in the FDCS ratios shown in figures 3.2 and 3.3 can now be understood. For ionization without excitation (figure 3.5), the 4DW model overestimates the CCC and DWB2-RMPS by roughly a factor of 2. For asymmetric energy with excitation (figures 3.6 and 3.7), the 4DW underestimates the experiment by about a factor of 2, and for symmetric energy gets the magnitudes correct. This results in the overestimation of the ratios by the 4DW and FBA models.

One might be puzzled that the 4DW predicts the magnitude of the n = 2 (n = 3) FDCS so much better for symmetric energy than asymmetric energy. This is not due entirely to the symmetric treatment of the outgoing electrons, but rather the exchange between the two continuum electrons in the final state. The complete FDCS should be calculated with both the direct and exchange amplitudes. The direct amplitude corresponds to the case where the scattered electron is the "fast" electron, and the exchange amplitude corresponds to the case where the scattered electron is the "slow" electron. For highly asymmetric energies, one typically expects that the exchange amplitude is quite small. Therefore, it is usually ignored, and is not included in either the FBA or 4DW calculations in the asymmetric energy cases. However, for the symmetric energy case, the direct and exchange amplitudes are identical and can both be included by simply calculating the direct amplitude and multiplying by 2, which is what has been done here. Therefore, exchange between the outgoing electrons is included for symmetric energy sharing, but not for asymmetric energy sharing.

To get an idea of the importance of exchange for the asymmetric case, a simple first order distorted wave Born approximation calculation for ionization without excitation using an uncorrelated product wave function for the helium atom was performed. This showed that inclusion of the exchange amplitude lowered the cross

section by about 20%, suggesting that exchange may be more important than one would typically expect for these kinematics.

3.2. SINGLE CHARGE TRANSFER

As discussed in Section 1.2, in proton + helium SC, an incident proton collides with a helium atom, captures a single electron, and leaves the collision as a neutral ground state hydrogen atom. The remaining electron in the He^+ ion is also left in the ground-state.

There is much experimental data available for single charge transfer, and the model used in these calculations is not new. However, the calculations were necessary for analysis with double charge transfer, and so are presented in figure 3.8 for the specific energies needed. FDCS are calculated using the 4BTE model discussed in Section 2.3.1. The calculation with all three terms in the perturbation is similar to a JS calculation, while the calculation without the nuclear term is similar to an OBK calculation. These results exhibit some well-known features and trends. The unphysical minimum seen in the calculation with the full perturbation is typically attributed to a cancellation of the terms in the perturbation [92]. Note that this minimum becomes deeper and shifts to smaller angles as the projectile energy increases, as was previously observed by Band et. al [189] and Sil et al. [190]. The removal of the projectile-nuclear term in the perturbation results in the removal of this minimum, and an increase in the overall magnitude of the cross section, something seen by Belkić and Salin [34].

3.3. TRANSFER-EXCITATION

The results of the 4BTE model, which was discussed in Section 2.3.1, are presented here for proton + helium TE. Currently, experimental data for fully differential cross sections are available for proton + helium TE collisions at projectile energies

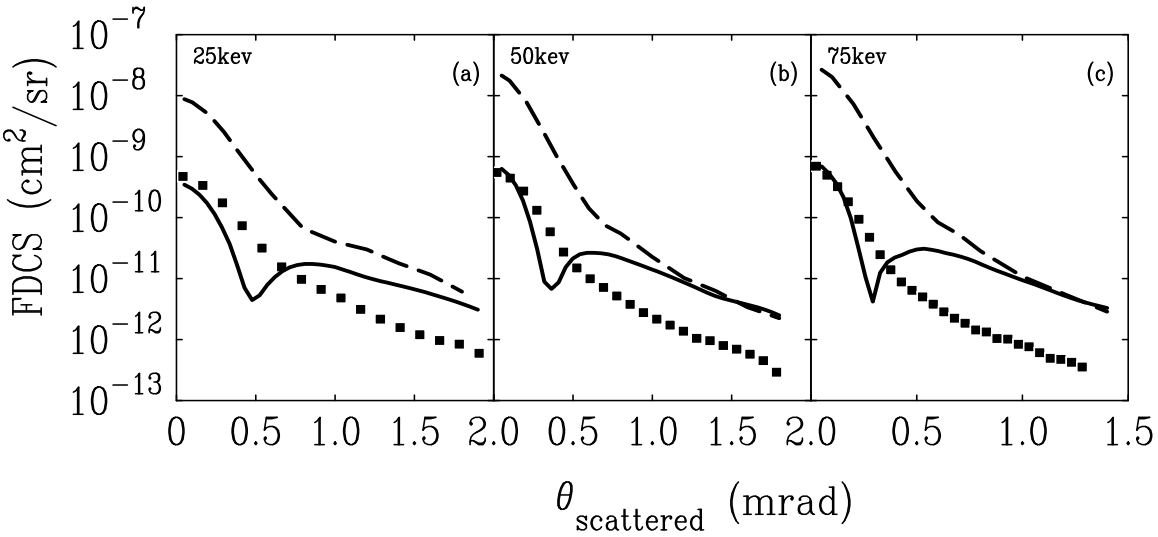

Figure 3.8. FDCS as a function of projectile scattering angle for p + He SC. Experiment: ■ results of Schulz et al. [172] for the incident projectile energies shown in the figure. Both theoretical curves are from the 4BTE model with a plane wave for the incident projectile, Hylleraas wave function for the helium atom, and a Coulomb wave for the scattered projectile. Theoretical results: — all three terms in the perturbation; - - - no projectile-nuclear term in the perturbation.

of 25, 50, and 75 keV. These energies correspond to projectile speeds of 1, 1.4, and 1.7 a.u., placing them at the lower end of the intermediate energy regime. The experiment was performed by Hasan et al. [168], and is absolute. From experiment, it is known that the outgoing hydrogen atom is in the ground state, and the residual helium ion is in an excited state. However, it is not known in which excited state the helium ion is left. Therefore, the cross sections must be summed over all possible excited states. Calculations have shown that contributions from excited states above n = 4 are negligible, as are contributions from higher angular momentum states. This can be seen in figure 3.9. Because of this, the present results include only s and p excited states for $2 \leq n \leq 4$.

Figures 3.10 and 3.11 show the effect of the projectile-atom interaction on the FDCS. Despite the fact that the target atom is neutral, the interaction of the

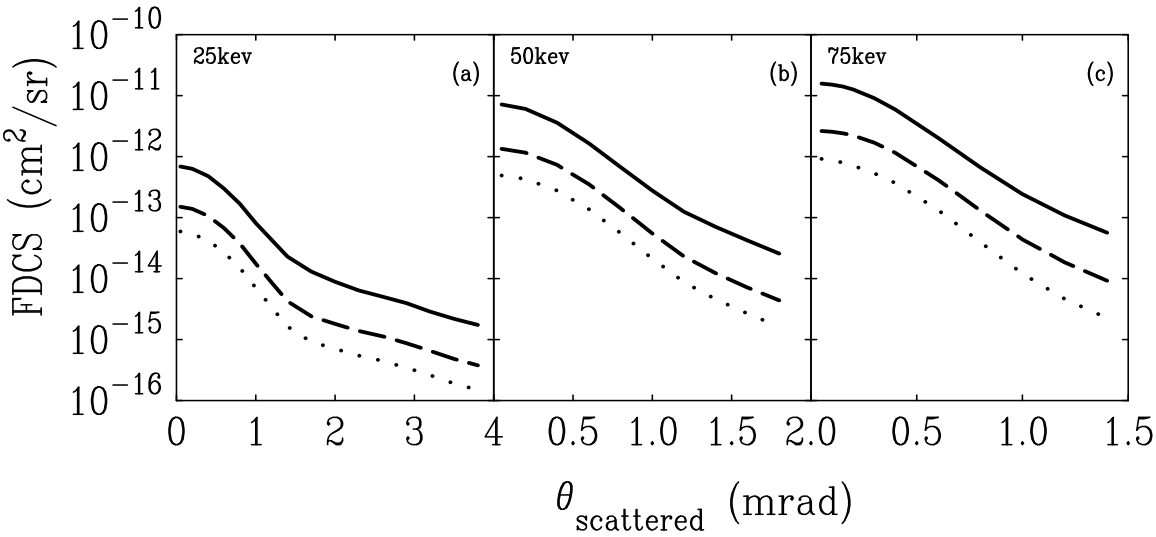

Figure 3.9. FDCS as a function of projectile scattering angle for p + He TE showing the relative magnitudes of excitation to different energy levels in the He^+ ion. All theoretical curves are from the 4BTE model with a plane wave for the incident projectile, Hylleraas wave function for the helium atom, and Coulomb wave for the scattered projectile. Theoretical results: — excitation to the n = 2 level; - - - excitation to the n = 3 level; $\cdots$ excitation to the n = 4 level.

projectile with the constituents of the target atom can be included through the use of an Eikonal initial state wave function. When the projectile is close to the target, its interaction with the nucleus and the atomic electrons is included through a phase factor modifying a plane wave. Figure 3.10 shows the effect of including the incident projectile-atom interaction when a plane wave is used for the scattered projectile. Similarly, figure 3.11 shows this effect when a Coulomb wave is used for the scattered projectile.

The Eikonal wave function is typically used for high energy projectiles, and is considered a valid approximation when the ratio Z_{nuc}/v_p is less than 1. For the three energies studied here, this ratio ranges between 1.2 (75 keV) and 2 (25 keV), pushing the limit of the Eikonal's validity. In both figures 3.10 and 3.11, the use of Eikonal wave function has a fairly small effect, with the largest difference being observed at

small scattering angles. The biggest change in shape occurs at 25 keV, where the Eikonal approximation is expected to be the least valid.

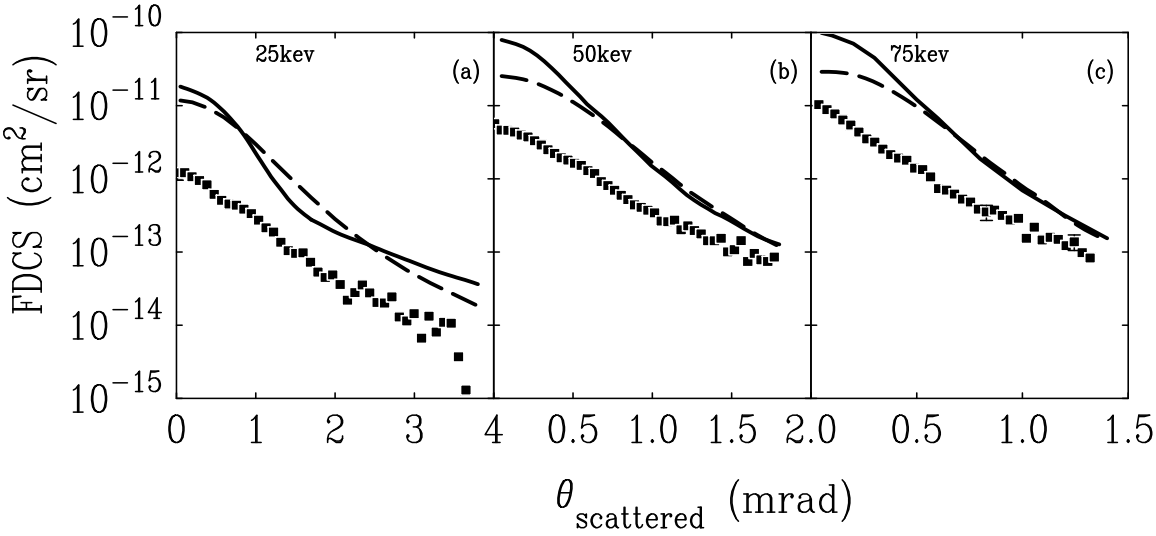

Figure 3.10. FDCS as a function of projectile scattering angle for p + He TE showing the effect of the incident projectile-target atom interaction. Experiment: ■ results of Hasan et al. [168] for the incident projectile energies shown in the figure. Theoretical results: — 4BTE model with an Eikonal wave function for the incident projectile, Hylleraas wave function for the helium atom, and plane wave for the scattered projectile; - - - 4BTE model with a plane wave for the incident projectile, Hylleraas wave function for the helium atom, and plane wave for the scattered projectile

In the final state, the outgoing hydrogen atom is in the field of the He^+ ion. Asymptotically, the ion has a charge of 1, but the hydrogen atom is neutral. This seems to imply that a plane wave should be used for the outgoing hydrogen in order to match asymptotic boundary conditions. However, the dynamics of the collision take place at small projectile-ion separations, so that one might consider the use of a Coulomb wave for the proton in the field of the He^+ ion (i.e. a Coulomb wave with charge 1). Results for both of these approximations are shown in figure 3.12. It is clear that the use of a Coulomb wave is required in order to achieve the correct order

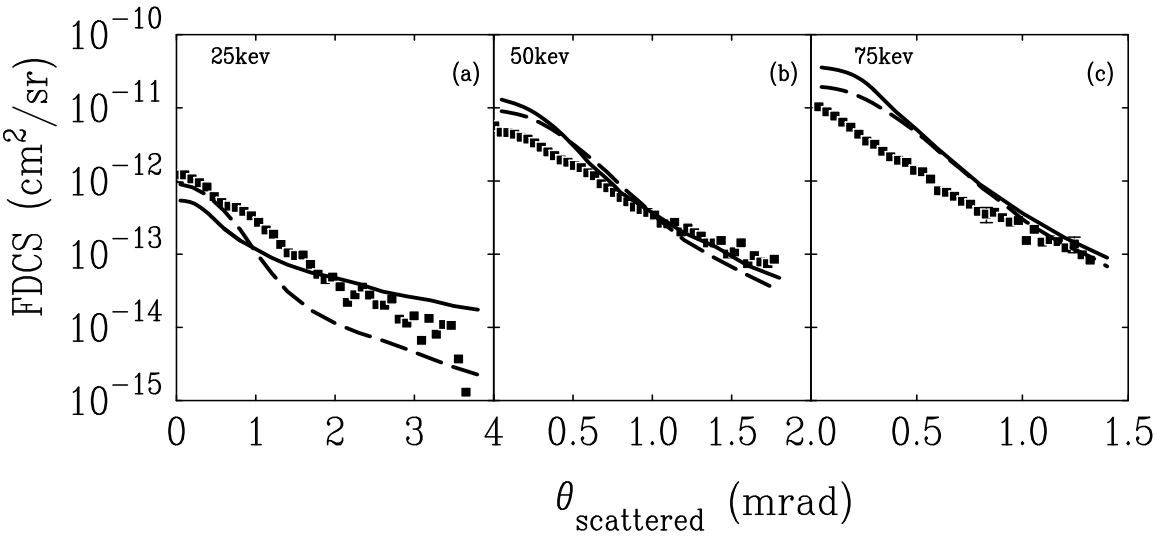

Figure 3.11. FDCS as a function of projectile scattering angle for p + He TE showing the effect of the incident projectile-target atom interaction. Experiment: ■ results of Hasan et al. [168] for the incident projectile energies shown in the figure. Theoretical results: — 4BTE model with an Eikonal wave function for the incident projectile, Hylleraas wave function for the helium atom, and Coulomb wave for the scattered projectile; - - - 4BTE model with a plane wave for the incident projectile, Hylleraas wave function for the helium atom, and Coulomb wave for the scattered projectile.

of magnitude. However, virtually no change in shape between the two calculations is observed. One might also notice that the difference between the calculations diminishes as projectile energy increases. This is expected since a projectile with a larger speed spends less time in the field of the ion than one with a smaller speed.

In figure 3.13, the effect of initial state correlation is shown. One would be inclined to think that correlation would play an important role in the first order model of a four body process because the only interactions included in the perturbation are between the projectile and each individual electron, as well as the projectile-nuclear interaction. Thus, in order for two electrons to change state, some correlation should be required. However, figure 3.13 shows this expectation to be incorrect.

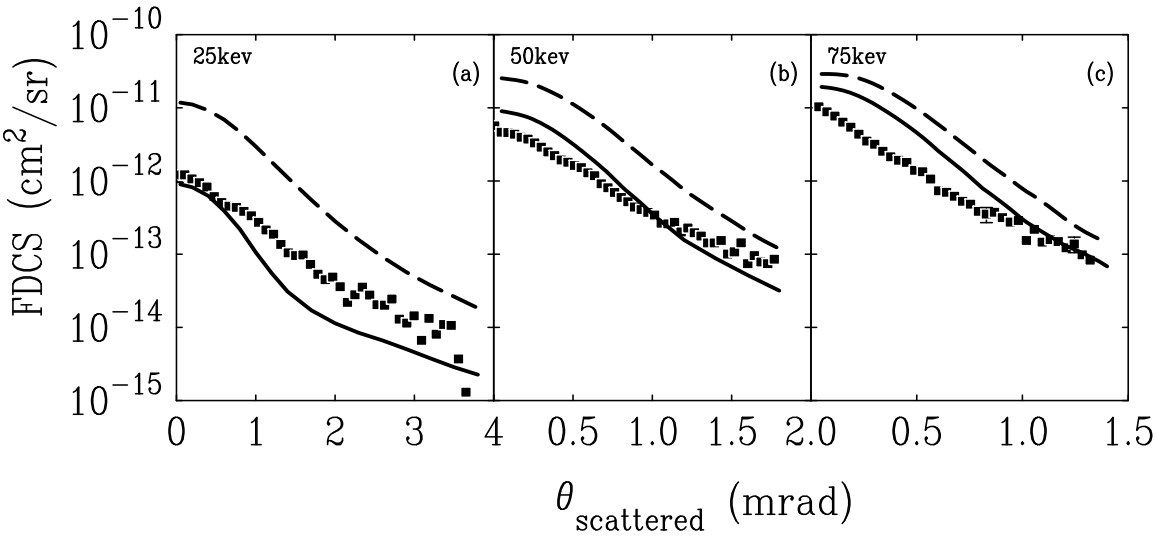

Figure 3.12. FDCS as a function of projectile scattering angle for p + He TE showing the effect of the scattered projectile-residual ion interaction. Experiment: ■ results of Hasan et al. [168] for the incident projectile energies shown in the figure. Theoretical results: — 4BTE model with a plane wave for the incident projectile, Hylleraas wave function for the helium atom, and Coulomb wave for the scattered projectile; - - - 4BTE model with a plane wave for the incident projectile, Hylleraas wave function for the helium atom, and plane wave for the scattered projectile.

Here, two different atomic helium wave functions are used. The Hartree-Fock wave function is a product wave function that treats the two atomic electrons independently with no correlation. This calculation corresponds to an independent particle model. The Hylleraas wave function includes both radial and angular correlation between the two initial state atomic electrons. There is very little difference between these calculations except at small scattering angles, indicating that correlation is not important in this process.

Figure 3.14 shows the effect of the projectile-nuclear interaction on the fully differential cross sections. This term in the potential corresponds to scattering from the nucleus. As noted in the Introduction, the FDCS at large angles should be dominated by this interaction. Thus, its exclusion from the calculation should result in a more rapid decrease of the FDCS as scattering angle increases. This effect is

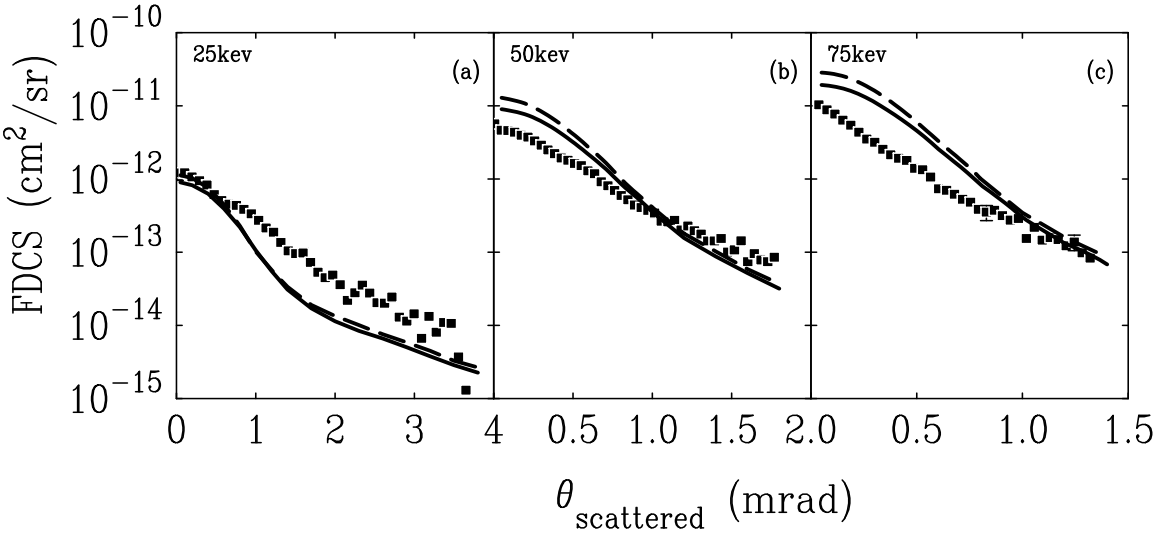

Figure 3.13. FDCS as a function of scattering angle for p + He TE showing the effect of electron correlation in the target atom wave function. Experiment: ■ results of Hasan et al. [168] for the incident projectile energies shown in the figure. Theoretical results: — 4BTE model with a plane wave for the incident projectile, Hylleraas wave function for the helium atom, and Coulomb wave for the scattered projectile; - - - 4BTE model with a plane wave for the incident projectile, Hartree-Fock wave function for the helium atom, and Coulomb wave for the scattered projectile.

not observed here. Also, contrary to SC, for TE, exclusion of this interaction has the effect of lowering the magnitude, but not drastically altering the shape.

3.4. DOUBLE CHARGE TRANSFER

In the DC process described in Section 1.3, an incident proton captures both atomic electrons from the target helium atom and leaves the collision as an H^- ion. Theoretical results using the 4BDC model discussed in Section 2.4.1 are presented in figure 3.15 for the same energies as SC and TE (25, 50, 75 keV). The first thing to note is that experimental results for DC are about three orders of magnitude smaller than those of SC, indicating a much less likely process. The second thing to note is the similarity of the DC differential cross section to the SC differential cross section.

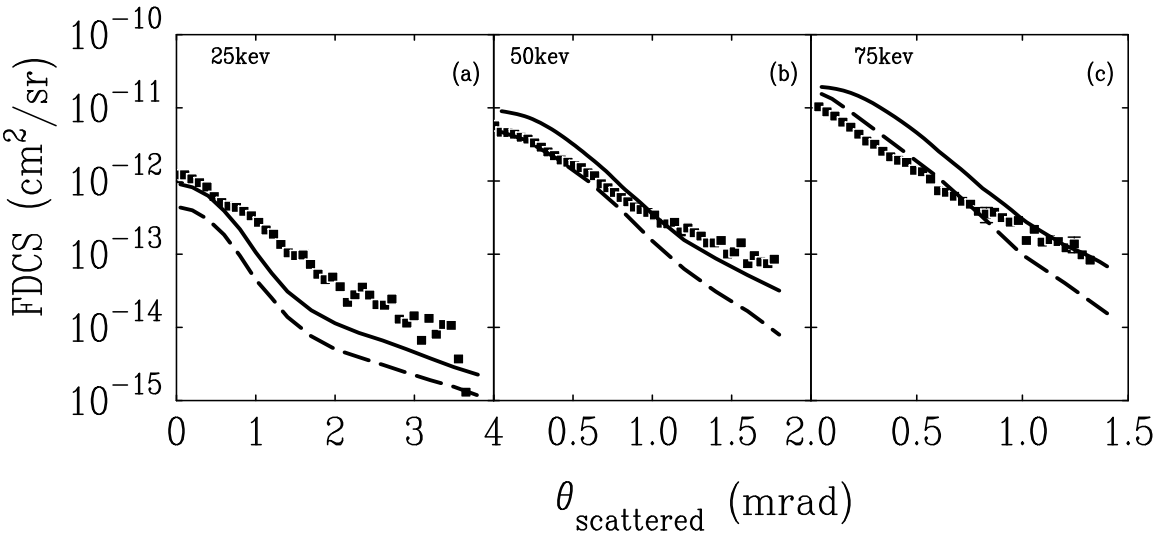

Figure 3.14. FDCS as a function of scattering angle for p + He TE showing the effect of the projectile-nuclear interaction. Experiment: ■ results of Hasan et al. [168] for the incident projectile energies shown in the figure. Both theoretical curves are from the 4BTE model with a plane wave for the incident projectile, Hylleraas wave function for the helium atom, and Coulomb wave for the scattered projectile. Theoretical results: — all three terms in the perturbation; - - - without the projectile-nuclear term in the perturbation.

A minimum is again observed in the DC cross section, and excluding the projectile-nuclear term from the perturbation results in the removal of this minimum. Also, the location of this minimum moves to smaller angles as energy increases. As is expected, theory requires the inclusion of the projectile-nuclear term to more accurately predict the magnitude of experiment. However, the models shown in figure 3.15 still overestimate experiment by a factor of 100.

The effect of angular correlation in both the initial and final states is shown in figure 3.16. Four calculations are shown, using either a 20 term Hylleraas wave function or an analytic Hartree-Fock wave function for the initial state helium atom. For the final state H^- ion, either a 20 term Hylleraas wave function or a two parameter variational wave function is used. All four of the calculations shown are similar in both shape and magnitude, indicating that angular correlation is not important in

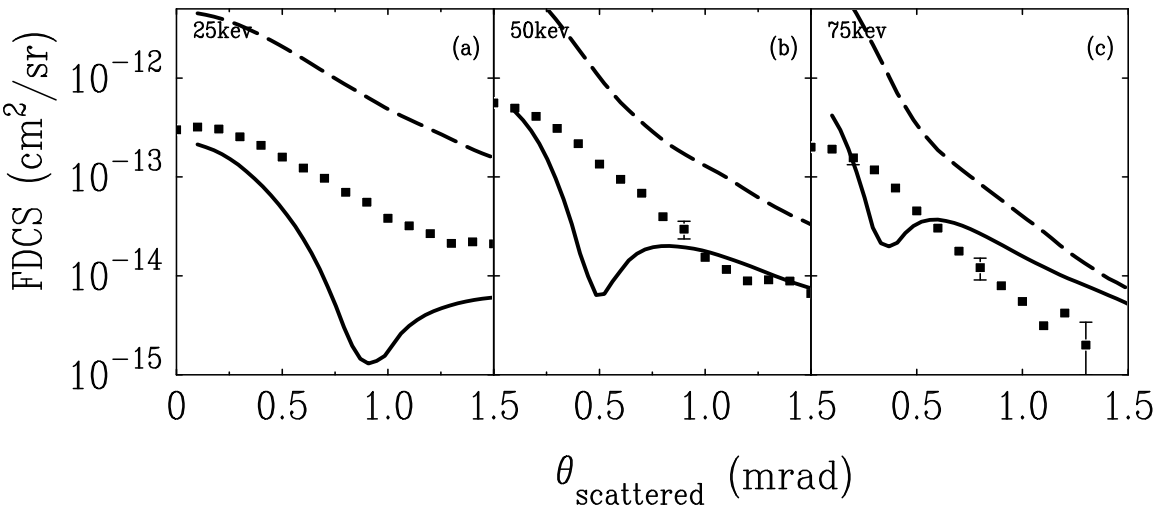

Figure 3.15. FDCS as a function of projectile scattering angle for p + He DC. Experiment: ■ results of Schulz et al. [172] for the incident projectile energies shown in the figure. Both theoretical curves are from the 4BTE model with a plane wave for the incident projectile, Hylleraas wave functions for the helium atom and H^- ion, and a Coulomb wave for the scattered projectile. Theoretical results: — all three terms in the perturbation; - - - without the projectile-nuclear term in the perturbation. Both calculations have been divided by 100.

the DC process. In the initial state helium atom, the inclusion of correlation slightly lowered the magnitude of the FDCS, while in the final state H^- ion, the inclusion of correlation slightly increased the magnitude of the FDCS.

Figure 3.17 shows the ratio of DC to SC, where some structure can be seen in the experiment. Clearly, since the absolute magnitude of the SC and DC theory is not in good agreement with experiment, the ratio results are not expected to have proper magnitude agreement either.

Structure is also predicted by theory, as well, and it can be traced to either the individual DC or SC results. For inclusion of the projectile-nuclear term, the large peak in the ratio at small angles is due to the minimum in the SC cross section. Also, the minimum in the ratio just to the right of the peak is due to the minimum in the DC cross section.

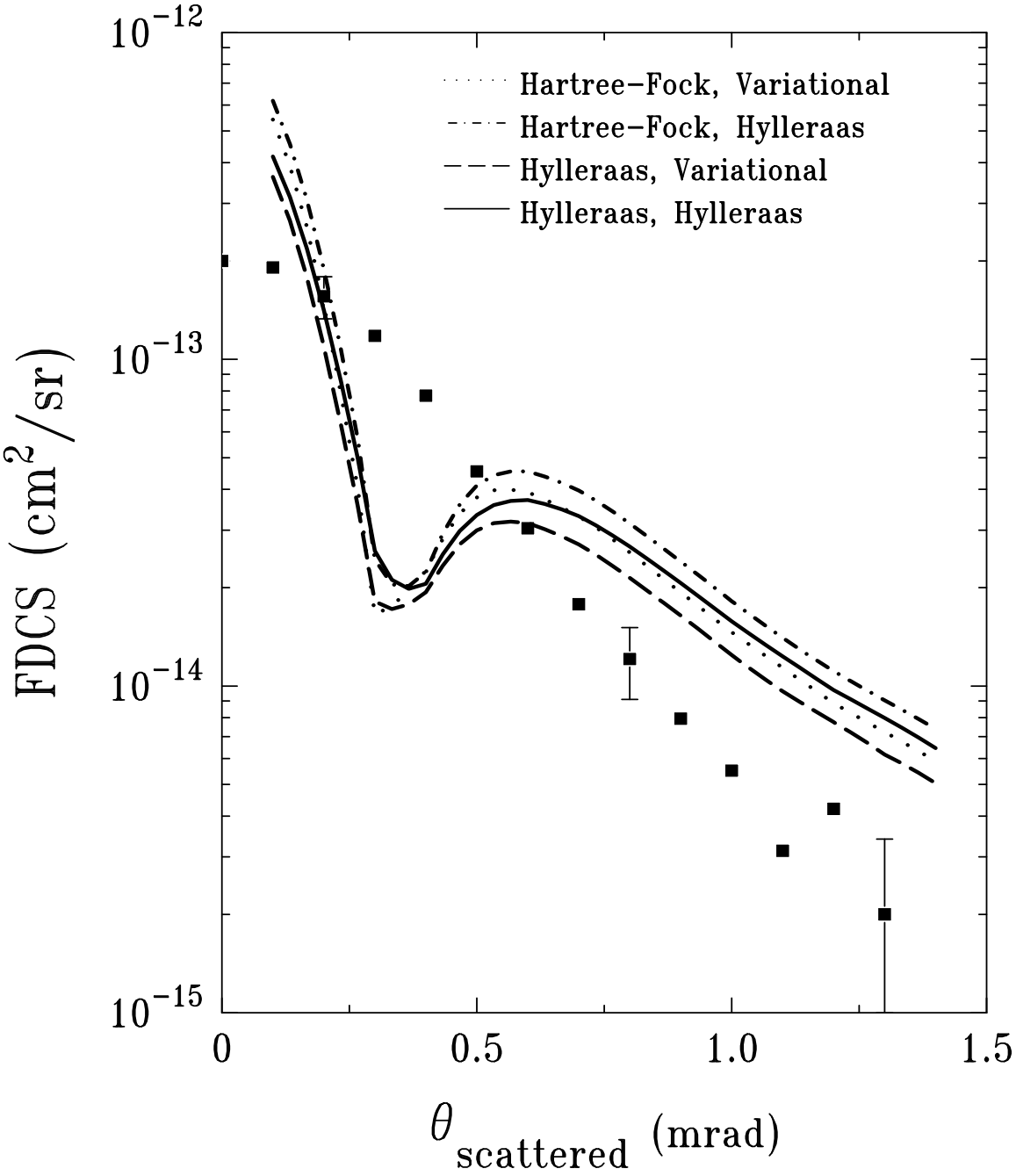

Figure 3.16. FDCS for 75 keV p + He DC showing the effect of electron correlation in the target atom and the scattered ion. Experiment: ■ results of Schulz et al. [172]. All calculations are the 4BTE model with a plane wave for the incident projectile and Coulomb wave for the scattered projectile. The labels in the figure indicate the helium atom and H^- wave functions respectively. All calculations have been divided by 100.

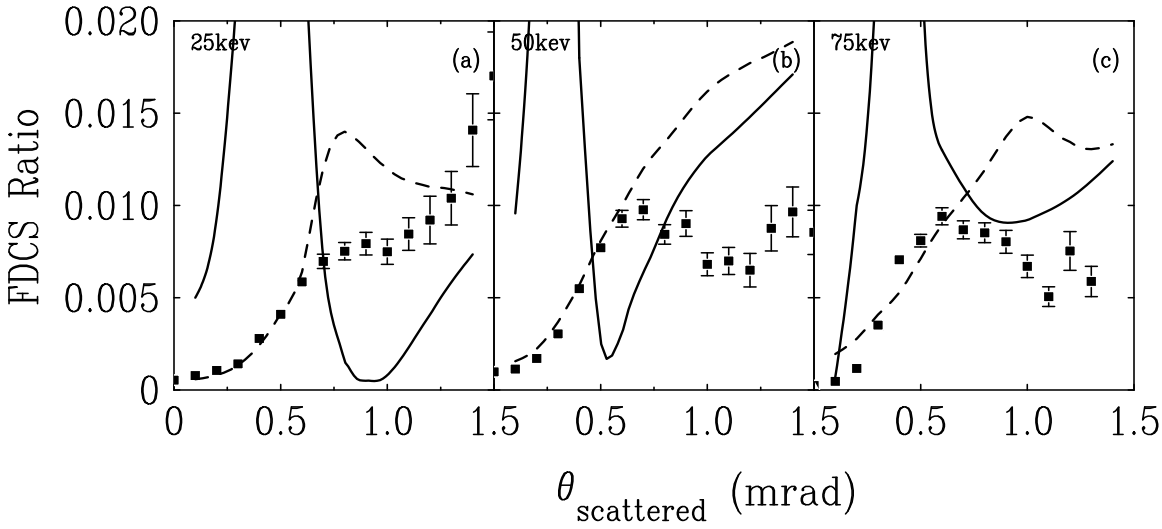

Figure 3.17. FDCS ratios for p + He DC divided by p + He SC. Experiment: ■ results of Schulz et al. [172] for the incident projectile energies shown in the figure. Both theoretical curves are from the 4BTE model with a plane wave for the incident projectile, Hylleraas wave functions for the helium atom and H^- ion, and a Coulomb wave for the scattered projectile. Theoretical results: — all three terms in the perturbation divided by (a) 100, (b) 35, (c) 25; - - - without the projectile-nuclear term in the perturbation divided by 10 in all three panels.

If the projectile-nuclear term is excluded, the shape of the ratio is in fair agreement with experiment. Here, however, it is not easy to identify the source of the structure. These ratios seem to imply that scattering from the nucleus should not be included in the theory. One possible explanation for this is that capture takes place at large impact parameters, and that the scattering is dominated by the projectile-electron interaction.

The results of the SC, TE, and DC calculations lead to some puzzling observations. First, the model correctly predicts the magnitude of the SC and TE results, but overestimates the DC results by a factor of 100. Second, the SC and DC calculations show a minimum when the full perturbation potential is used, but no minimum when the projectile-nuclear term is removed. Also, for the SC and DC calculations, removal of the projectile-nuclear term increases the magnitude of the calculation. However,

for TE, there is no minimum when the full perturbation is used, and removing the projectile-nuclear term has little effect on the shape or magnitude of the calculation. This indicates that a cancellation of terms in the perturbation cannot be the only explanation for the minimum seen in the SC and DC cross sections.

4. CONCLUSION

In an attempt to improve the understanding of four-body collision processes, several four-body models have been presented and compared to experiment in the context of fully differential cross sections (FDCS). For the case of excitation-ionization (EI), the Four-Body Distorted Wave (4DW) and First Born Approximation (FBA) models were presented, and the effects of projectile interactions were explored. Through the use of distorted waves, the 4DW model contains elastic scattering of the projectile from the target to infinite order in both the initial and final state. The FBA neglects this interaction. It was found that the importance of these interactions depends upon the kinematics. For smaller projectile energies, a distorted wave treatment was necessary to achieve the correct shape. However, for larger projectile energies, the difference between a plane wave and a distorted wave treatment was small.

In addition to elastic scattering, the 4DW model also includes the post-collision interaction (PCI) to infinite order, while the FBA model neglects PCI. PCI accounts for the mutual repulsion of the two outgoing electrons in the final state. In all cases, the inclusion of PCI improves agreement with experiment by shifting the theoretical peak locations closer to the experimental locations. PCI was found to be particularly important for the case of symmetric energy sharing since the two outgoing electrons leave with the same speed and have a greater effect on each other.

There are four main possibilities for the remaining discrepancies between experiment and the 4DW model for EI. The first is an inadequate treatment of the ejected electron-residual ion interaction. While the 4DW model treats this interaction through the use of a distorted wave, this may be inadequate for ejected electron energies less than 10 eV, where exchange between the ejected and bound electrons is more likely. This is the kinematical situation for the relative experimental results presented in Section 3.1.1, and the likely cause for any disagreement between this experiment and theory. The second possibility is that exchange between the projectile

electron and remaining He^+ bound electron is not negligible. For highly asymmetric energy sharing, the probability of this type of exchange is typically thought to be small. However, for the kinematics used in the FDCS ratios and absolute FDCS shown in Sections 3.1.2 and 3.1.3, the energies may not be asymmetric enough, and exchange may be important. For symmetric energy sharing this exchange was included, and improved agreement in magnitude was observed.

The third possibility for the discrepancies between experiment and the 4DW model is the large scattering angles involved. It has been seen with similar models that as the scattering angle increases, the shape agreement between experiment and theory is maintained, but the magnitude of the theory decreases. The same effect was observed here, where the 4DW generally agreed well with the shape of experiment, but incorrectly predicted the magnitude. The fourth possibility for the remaining disagreement between experiment and theory is that a second, or higher, order model is necessary to describe this process. Because EI is a four-body process in which two atomic electrons change state, it is not unreasonable to expect that a model that includes projectile-electron interactions to the second, or higher, order might be required.

Aside from the EI process, the remaining collisions studied in Sections 3.2 - 3.4 involve heavy particle scattering and charge transfer. The single capture (SC) and transfer-excitation (TE) processes are similar, and in fact were studied using the same Four-Body Transfer-Excitation (4BTE) model. The difference between these two processes is simply in which state the residual ion is left. However, great differences were observed in the calculations for SC and TE. In particular, for SC, a pronounced minimum was observed when the full perturbation was used. This minimum was removed when the projectile-nuclear interaction was excluded from the perturbation. These results were expected since they have been seen in similar models. However, for TE, no such minimum was observed and the removal of the projectile-nuclear term

from the perturbation had little effect on the FDCS. The accepted explanation for the appearance of a minimum when the full perturbation potential is used is that it is a result of cancellation of the terms in the perturbation. If this is indeed the case, one would expect the same to be true of TE, where the only thing that has changed is the state of the residual ion. Since no minimum is observed for TE, a cancellation of terms alone cannot account for the minimum.

In addition to studying the effect of the projectile-nuclear interaction, the projectile-atom and projectile-ion interactions were studied in the initial and final states respectively. For the projectile-atom interaction, an Eikonal wave function was used to include distortion of the incident projectile wave function by the target atom. This distortion had little effect on the FDCS, indicating that the projectile-atom interaction is not important in the TE process. In the final state, the use of a Coulomb wave for the scattered projectile was necessary to achieve the correct order of magnitude, with the effect of the Coulomb wave diminishing as projectile energy increased.

The effect of electron correlation in the target helium atom was also studied. It was expected that this interaction would be important in causing both atomic electrons to change state. However, this expectation was incorrect, and it was shown that the effect of correlation was negligible in the TE process.

Double capture (DC) was the final collision process studied through the development of the Four-Body Double Capture (4BDC) model. Like the theoretical SC results, the 4BDC model predicts a minimum in the FDCS when the full perturbation is used. Again, this minimum is removed when the projectile-nuclear term is excluded from the perturbation. In addition to the puzzling nature of the minimum, it is interesting that the 4BTE model correctly predicts the magnitude of the SC and TE experiment, but the 4BDC model overestimates the experiment by a factor of

100. The effect of electron correlation was shown to have little effect in either the initial or final state of the DC process.

The final analysis made for charge transfer was to examine the ratio of FDCS for DC divided by SC. The ratio calculated with results that neglected the projectile-nuclear term in the perturbation agreed best with experiment, primarily because they did not exhibit the unphysical minimum in the individual FDCS. However, these results overestimated the magnitude of the ratios, and did not exhibit the structure seen in experiment.

The models and results presented here represent a step forward in the study of four-body collision processes. They are unique in their ability to explicitly treat all four particles in the collision, and to study the individual two particle interactions. However, the four-body problem remains a difficult one both theoretically and experimentally. Current agreement between experiment and theory is generally fair, and it is anticipated that as computational resources and experimental technology improve, the remaining discrepancies will be explained.

APPENDIX A

ATOMIC UNITS

In atomic units,

$$a_0 = 1 \tag{A.1}$$

$$\hbar = 1 \tag{A.2}$$

$$m_e = 1 \tag{A.3}$$

$$\frac{e^2}{4\pi\epsilon_0} = 1. \tag{A.4}$$

$$\tag{A.5}$$

Also, 1 a.u. of energy is equivalent to 27.2 eV, and the fine structure constant is given by

$$\alpha = \frac{e^2}{4\pi\epsilon_0\hbar c} = \frac{1}{137}. \tag{A.6}$$

APPENDIX B

CALCULATION OF THE FINAL STATE PERTURBATION

Within the two potential formulation of Section 2.1.4, the post form of the exact transition matrix is given by [175]

$$T_{fi} = \langle \Psi_f^{(-)} \mid W_f^\dagger \mid \Psi_i \rangle + \langle \Psi_f^{(-)} \mid V_i - W_f^\dagger \mid \beta_{\vec{k}_i} \xi_{He} \rangle, \tag{B.1}$$

where Ψ_i is the total initial state wave function, which includes the Eikonal approximation for the incident projectile, $\Psi_f^{(-)}$ is the final state wave function, $\beta_{\vec{k}_i}$ is a plane wave, and ξ_{He} is the initial state helium wave function. The initial state proton-helium interaction V_i is given by equation (124). The final state perturbation W_f satisfies

$$(H - E)\Psi_f^{(-)} = W_f \Psi_f^{(-)}, \tag{B.2}$$

where H is the full Hamiltonian

$$H = -\frac{1}{2\mu_{pa}}\nabla_{r_1}^2 - \frac{1}{2}\nabla_{r_2}^2 - \frac{1}{2}\nabla_{r_3}^2 + V, \tag{B.3}$$

and E is the total center of mass energy

$$E = \frac{k_f^2}{2\mu_{pa}} + B_H + B_{He^+}. \tag{B.4}$$

The quantities B_H and B_{He^+} are the binding energies of the hydrogen atom and He^+ ion respectively. Let V be the total interaction potential for a proton + helium collision, such that

$$V = \frac{2}{r_1} - \frac{2}{r_2} - \frac{2}{r_3} - \frac{1}{r_{12}} - \frac{1}{r_{13}} + \frac{1}{r_{23}}.$$

The perturbation W_f can then be calculated by

$$W_f = \frac{1}{\Psi_{\vec{k}_f}^{(-)}}(H - E)\Psi_{\vec{k}_f}^{(-)} \tag{B.5}$$

The final state wave function $\Psi^{(-)}_{\vec{k}_f}$ is written as a product of the wave functions for the three particles relative to the helium nucleus

$$\Psi^{(-)}_{\vec{k}_f} = A(\vec{r}_1)B(\vec{r}_3)C(\vec{r}_{12}). \tag{B.6}$$

For the case of transfer-excitation, $A(\vec{r}_1)$ is the scattered projectile wave function, $B(\vec{r}_3)$ is the He^+ bound state wave function, and $C(\vec{r}_{12})$ is the hydrogen wave function. The He^+ bound state wave function and hydrogen wave functions are given by

$$B(\vec{r}_3) = \psi_{He^+}(\vec{r}_3) \tag{B.7}$$

and

$$\begin{aligned} C(\vec{r}_{12}) &= \phi_H(\vec{r}_{12}) \\ &= \frac{e^{-r_{12}}}{\sqrt{\pi}}. \end{aligned} \tag{B.8}$$

The scattered projectile wave function can be either a plane wave given by equation (13)

$$A(\vec{r}_1) = \beta_{\vec{k}_f}(\vec{r}_1) = \frac{e^{i\vec{k}_f\cdot\vec{r}_1}}{(2\pi)^{3/2}} \tag{B.9}$$

or a Coulomb wave given by equation (35)

$$A(\vec{r}_1) = \frac{Ne^{i\vec{k}_f\cdot\vec{r}_1}}{(2\pi)^{3/2}}\, {}_1F_1(-i\gamma, 1; ik_f r_1 + i\vec{k_f}\cdot\vec{r_1}), \tag{B.10}$$

with $N = e^{-\pi\gamma/2}\Gamma(1+i\gamma)$, $\gamma = \frac{\mu_{pt} Z_{He^+} Z_p}{k_1}$, and ${}_1F_1(-i\gamma, 1; ik_f r_1 + i\vec{k_f}\cdot\vec{r_1})$ a confluent hypergeometric function. The left hand side of equation (B.2) can then be written as

$$\begin{aligned}(H-E)\Psi_f &= -\frac{B}{2\mu_{pa}}\nabla^2_{r_1}(AC) - \frac{AB}{2}\nabla^2_{r_2}C - \frac{AC}{2}\nabla^2_{r_3}B \\ &\quad +(\frac{2}{r_1} - \frac{2}{r_2} - \frac{2}{r_3} - \frac{1}{r_{12}} - \frac{1}{r_{13}} + \frac{1}{r_{23}})ABC \\ &\quad -\frac{k_f^2}{2\mu_{pa}}ABC - B_H ABC - B_{He^+}ABC.\end{aligned} \tag{B.11}$$

Note that

$$-\frac{1}{2}\nabla^2_{r_3}B - \frac{2}{r_3}B = B_{He^+}B \tag{B.12}$$

and

$$-\frac{1}{2}\nabla^2_{r_{12}}C - \frac{2}{r_{12}}C = B_H C. \tag{B.13}$$

Also, because $C(\vec{r}_{12})$ is only a function of $\vec{r}_{12}$,

$$\nabla^2_{r_{12}}C = \nabla^2_{r_1}C = \nabla^2_{r_2}C. \tag{B.14}$$

Then, equation (B.11) can be written as

$$\begin{aligned}(H-E)\Psi_f &= -\frac{B}{2\mu_{pa}}\nabla^2_{r_1}(AC) + (\frac{2}{r_1} - \frac{2}{r_2} - \frac{1}{r_{13}} + \frac{1}{r_{23}})ABC \\ &\quad -\frac{k_f^2}{2\mu_{pa}}ABC.\end{aligned}$$

Using the operator identity $\nabla^2_{r_1}(AC) = C\nabla^2_{r_1}A + A\nabla^2_{r_1}C + 2\nabla_{r_1}A\cdot\nabla_{r_1}C$ gives

$$\begin{aligned}(H-E)\Psi_f &= -\frac{B}{2\mu_{pa}}[C\nabla^2_{r_1}A + A\nabla^2_{r_1}C + 2\nabla_{r_1}A\cdot\nabla_{r_1}C] \\ &\quad +(\frac{2}{r_1} - \frac{2}{r_2} - \frac{1}{r_{13}} + \frac{1}{r_{23}})ABC - \frac{k_f^2}{2\mu_{pa}}ABC.\end{aligned}$$

Then, the perturbation W_f can be written as

$$\begin{aligned} W_f &= -\frac{1}{2\mu_{pa}A}\nabla^2_{r_1}A - \frac{1}{2\mu_{pa}C}\nabla^2_{r_1}C - \frac{1}{\mu_{pa}AC}\nabla_{r_1}A\cdot\nabla_{r_1}C \\ &\quad +(\frac{2}{r_1}-\frac{2}{r_2}-\frac{1}{r_{13}}+\frac{1}{r_{23}}) - \frac{k_f^2}{2\mu_{pa}}. \end{aligned} \tag{B.15}$$

Using a plane wave for the scattered projectile gives

$$\nabla^2_1 e^{i\vec{k}_f\cdot\vec{r}_1} = -k_f^2 e^{i\vec{k}_f\cdot\vec{r}_1} \tag{B.16}$$

and

$$\nabla_1 e^{i\vec{k}_f\cdot\vec{r}_1} = i\vec{k}_f e^{i\vec{k}_f\cdot\vec{r}_1}. \tag{B.17}$$

Also, for SC or TE,

$$\nabla^2_{r_1} e^{-r_{12}} = \frac{r_{12}-2}{r_{12}} e^{-r_{12}}. \tag{B.18}$$

Plugging these into equation (B.15) gives the final state perturbation when treating the scattered projectile as a plane wave

$$W_f^{PW} = \frac{2-r_{12}}{2\mu_{pa}r_{12}} + i\frac{\vec{k_f}\cdot\vec{r_{12}}}{\mu_{pa}r_{12}} + (\frac{2}{r_1}-\frac{2}{r_2}-\frac{1}{r_{13}}+\frac{1}{r_{23}}).$$

Using a Coulomb wave for the scattered projectile gives

$$\nabla^2_1[{}_1F_1(i\gamma,1;-ik_fr_1+i\vec{k}_f\cdot\vec{r}_1)e^{i\vec{k}_f\cdot\vec{r}_1}] = \tag{B.19}$$

$$e^{i\vec{k}_f\cdot\vec{r}_1}[\frac{2\gamma k_f}{r_1}\,{}_1F_1(1+i\gamma,1;-ik_fr_1+i\vec{k}_f\cdot\vec{r}_1) \tag{B.20}$$

$$+2i\gamma k_f\,{}_1F_1(1+i\gamma,2;-ik_fr_1+i\vec{k}_f\cdot\vec{r}_1)(\widehat{k}_f+\widehat{r}_1)\cdot\vec{k}_f \tag{B.21}$$

$$-k_f^2\,{}_1F_1(i\gamma,1;-ik_fr_1+i\vec{k}_f\cdot\vec{r}_1)] \tag{B.22}$$

and

$$\nabla_1[{}_1F_1(i\gamma,1;-ik_f r_1+i\vec{k}_f\cdot\vec{r}_1)e^{i\vec{k}_f\cdot\vec{r}_1}]= \tag{B.23}$$

$$e^{i\vec{k}_f\cdot\vec{r}_1}[\gamma k_f {}_1F_1(1+i\gamma,2;-ik_f r_1+i\vec{k}_f\cdot\vec{r}_1)(\widehat{k}_f+\widehat{r}_1) \tag{B.24}$$

$$+i\,{}_1F_1(1+i\gamma,1;-ik_f r_1+i\vec{k}_f\cdot\vec{r}_1)\vec{k}_f]. \tag{B.25}$$

Thus, the final state perturbation when treating the scattered projectile as a Coulomb wave is given by

$$\begin{aligned} W_f^{CW} &= -\frac{\gamma k_f}{\mu_{pa}}\frac{{}_1F_1(1+i\gamma,1;-ik_f r_1+i\vec{k}_f\cdot\vec{r}_1)}{{}_1F_1(i\gamma,1;-ik_f r_1+i\vec{k}_f\cdot\vec{r}_1)} \\ &\quad+\frac{{}_1F_1(1+i\gamma,2;-ik_f r_1+i\vec{k}_f\cdot\vec{r}_1)}{{}_1F_1(i\gamma,1;-ik_f r_1+i\vec{k}_f\cdot\vec{r}_1)} \\ &\quad\times[\frac{\gamma k_f}{\mu_{pa}}(\widehat{k}_f+\widehat{r}_1)\cdot\frac{\vec{r}_{12}}{r_{12}}-i\frac{\gamma k_f}{\mu_{pa}}\vec{k}_f\cdot(\widehat{k}_f+\widehat{r}_1)] \\ &\quad+\frac{2-r_{12}}{r_{12}}+(\frac{2}{r_1}-\frac{2}{r_2}-\frac{1}{r_{13}}+\frac{1}{r_{23}})+i\frac{\vec{k}_f\cdot\vec{r}_{12}}{\mu_{pa}r_{12}}. \end{aligned} \tag{B.26}$$

APPENDIX C

EIKONAL WAVEFUNCTION FOR TWO ACTIVE ELECTRONS

The Eikonal wavefunction for a projectile incident on a one active electron atom is given by [183]

$$\psi^{1active} = \frac{e^{i\vec{k_i}\cdot\vec{r_1}}}{(2\pi)^{3/2}} \exp\left[i\frac{Z_p}{v_p}\ln\left(\frac{(v_p r_1 - \vec{v_p}\cdot\vec{r_1})}{(v_p r_{12} - \vec{v_p}\cdot\vec{r_{12}})}\right)\right], \tag{C.0}$$

where Z_p is the charge of the projectile and v_p is the speed of the incident projectile. Generalizing this to two active electrons gives

$$\begin{aligned}\psi^{2active} &= \chi\frac{e^{i\vec{k_i}\cdot\vec{r_1}}}{(2\pi)^{3/2}} \\ &= \frac{e^{i\vec{k_i}\cdot\vec{r_1}}}{(2\pi)^{3/2}} \exp\left[i\frac{Z_p}{v_p}\ln\left(\frac{(v_p r_1 - \vec{v_p}\cdot\vec{r_1})^{Z_{nuc}}}{(v_p r_{12} - \vec{v_p}\cdot\vec{r_{12}})(v_p r_{13} - \vec{v_p}\cdot\vec{r_{13}})}\right)\right].\end{aligned}$$

APPENDIX D

CODE TESTING

All calculations for this work were performed using FORTRAN codes that require nine-dimensional integrals. The excitation-ionization work used the *4dw.f* code; the transfer-excitation and single charge transfer work used the *transfer.f* code; and the double charge transfer work used the *transfer.double.capture.f* code. In order to ensure that the codes were functioning properly, numerous tests were completed.

D.1. *4DW.F*

The *4dw.f* code was checked by comparing results to those obtained from the *fba.f* code, which had been checked using analytic calculations. In one such test, the following integral was used:

$$\int\int\int \beta^{*}_{\vec{k}_f}\left(\vec{r}_1\right)\chi^{*}_{e}\left(\vec{r}_2\right)\varphi^{*}_{2p0}\left(\vec{r}_3\right)V_i\beta_{\vec{k}_i}\left(\vec{r}_1\right)\xi\left(\vec{r}_2,\vec{r}_3\right)d\vec{r}_1 d\vec{r}_2 d\vec{r}_3, \tag{D.0}$$

where $\beta_{\vec{k}_f,\,\vec{k}_i}$ is a plane wave given by equation (13), $\chi_e\left(\vec{r}_2\right)$ is the ejected electron wave function, $\xi(\vec{r}_2,\vec{r}_3)$ is the helium atom wave function, and V_i is the projectile-atom interaction given by equation (124). For energies of $\mathrm{E}_0 = 5500$ eV and $\mathrm{E}_2 = 75$ eV, and a scattering angle of 1°, the *4dw.f* and *fba.f* results differed by 0.9%.

To check that the PCI was correct, a calculation was performed for both the scattered and ejected electron leaving the collision with the same angle and energy. Since two electrons cannot be in the same place, the inclusion of PCI should cause the FDCS to be zero. The result from the code was numerically zero.

D.2. *TRANSFER.F*

The *transfer.f* code was checked by comparing results to analytic calculations, and to results from the code *4dw.f*. Table D.1 shows the analytic tests and the integrand used in each test. Table D.2 shows the tests performed for comparison with the *4dw.f* code and the integrand used in each test. The integrals performed

were

$$\int\int\int integrand\ d\vec{r}_1 d\vec{r}_2 d\vec{r}_3, \tag{D.0}$$

where the $d\vec{r}_1$ integral is performed in cylindrical coordinates, and the $d\vec{r}_2$ and $d\vec{r}_3$ integrals are performed in spherical coordinates. The analytic and numerical answers listed are the corresponding square of the T-Matrix, i.e. $\left|\int\int\int integrand\ d\vec{r}_1 d\vec{r}_2 d\vec{r}_3\right|^2$. In all cases, the initial state wave function used was

$$\xi_i(\vec{r}_2, \vec{r}_3) = \frac{\alpha^3}{\pi} e^{-\alpha(r_2+r_3)}, \tag{D.0}$$

where $\alpha = 1.6875$. The wave function ϕ_{nlm} is a hydrogenic wave function for the corresponding excited state. If no excited state is included as a subscript, multiple excited states were tested. The wave function β is a plane wave given by equation (13), χ_{CW} is a Coulomb wave function given by equation (143), and χ_{DW} is a numerical Hartree-Fock distorted wave.

Table D.1. Results of analytic code checking for *transfer.f* code.

Integrand	Analytic Answer	Numerical Answer	% difference
$\xi_i(\vec{r}_2, \vec{r}_3)\phi_{1s}(\vec{r}_3)/\rho_1$	3.233×10^7	3.232×10^7	0.03
$2\xi_i(\vec{r}_2, \vec{r}_3)\phi_{1s}(\vec{r}_3)/r_1$	8.052×10^7	8.021×10^7	0.2
$\xi_i(\vec{r}_2, \vec{r}_3)\phi_{1s}(\vec{r}_3)(\rho_1 + iz_1^2)$	4.917×10^{11}	4.929×10^{11}	0.1
$\xi_i(\vec{r}_2, \vec{r}_3)\phi_{1s}(\vec{r}_3)(\frac{1}{r_1} - \frac{1}{r_{12}})e^{i(\vec{k}_i-\vec{k}_f)\cdot\vec{r}_1}$	3551	3469	2.3
$\xi_i(\vec{r}_2, \vec{r}_3)\phi_{1s}(\vec{r}_3)(\frac{1}{r_1} - \frac{1}{r_{13}})e^{i(\vec{k}_i-\vec{k}_f)\cdot\vec{r}_1}$	240.2	235.7	1.9
$\beta_f^*(\vec{r}_1)\phi_{1s}^*(\vec{r}_3)V_i\beta_i(\vec{r}_1)\xi_i(\vec{r}_2, \vec{r}_3)$	6819	6717	1.4
$\beta_f^*(\vec{r}_1)\phi_{1s}^*(\vec{r}_3)\phi_{1s}^*(\vec{r}_2)V_i\beta_i(\vec{r}_1)\xi_i(\vec{r}_2, \vec{r}_3)$	24.22	24.21	0.04
$\beta_f^*(\vec{r})\beta_e^*(\vec{r}_3)\phi_{1s}^*(\vec{r}_2)V_i\beta_i(\vec{r}_1)\xi_i(\vec{r}_2, \vec{r}_3)$	3386	3297	2.5
$\beta_f^*(\vec{r}_1)\phi_{1s}^*(\vec{r}_{12})(-\frac{1}{r_{12}})\beta_i(\vec{r}_1)\xi_i(\vec{r}_2, \vec{r}_3)$	1.117×10^5	1.150×10^5	3.3
$\beta_f^*(\vec{r}_1)\phi_{1s}^*(\vec{r}_3)\phi_{1s}^*(\vec{r}_{12})(-\frac{1}{r_{12}})\beta_i(\vec{r}_1)\xi_i(\vec{r}_2, \vec{r}_3)$	2613	2700	3.4

Table D.2. Results of numerical code checking for *transfer.f* code.

Integrand	*4dw.f*	*transfer.f*	% difference
$\beta_f^*(\vec{r}_1)\beta_e^*(\vec{r}_2)\phi^*(\vec{r}_3)V_i\beta_i(\vec{r}_1)\xi_i(\vec{r}_2,\vec{r}_3)$	8249	8355	1.3
$\chi_{CWf}^*(\vec{r}_1)\beta_e^*(\vec{r}_2)\phi^*(\vec{r}_3)V_i\beta_i(\vec{r}_1)\xi_i(\vec{r}_2,\vec{r}_3)$	4886	4829	1.2
$\chi_{CWf}^*(\vec{r}_1)\chi_{DWe}^*(\vec{r}_2)\phi_{1s}^*(\vec{r}_3)V_i\beta_i(\vec{r}_1)\xi_i(\vec{r}_2,\vec{r}_3)$	4121	4122	0.02
$\beta_f^*(\vec{r}_1)\beta_e^*(\vec{r}_2)\phi_{1s}^*(\vec{r}_3)C(\vec{r}_{13})V_i\beta_i(\vec{r}_1)\xi_i(\vec{r}_2,\vec{r}_3)$	1266	1272	0.4
$\chi_{CWf}^*(\vec{r}_1)\beta_e^*(\vec{r}_3)\phi_{1s}^*(\vec{r}_{12})V_i\beta_i(\vec{r}_1)\xi_i(\vec{r}_2,\vec{r}_3)$	2.147×10^4	2.148×10^4	0.05

D.3. *TRANSFER.DOUBLE.CAPTURE.F*

This code is nearly identical to the *transfer.f* code. The only change made was to replace the He^+ and $H(1s)$ wavefunctions by an H^- wavefunction. Thus, all of the checks performed above still apply for this code, and no further testing was required. To ensure that the H^- wavefunctions were correct and properly normalized, their squares were integrated giving 0.8676 and 0.9453 for the Hartree-Fock and Hylleraas wavefunctions respectively.

BIBLIOGRAPHY

[1] H. Geiger and E. Marsden, *Proc. R. Soc. London* **82**, 495 (1909).

[2] E. Rutherford, *Philos. Mag.* 21, **669** (1911).

[3] A.S. Kheifets and I. Bray, *J. Phys. B: At. Mol. Opt. Phys.* **31**, L447 (1998).

[4] L. Malegat, P. Selles, and A.K. Kazansky, *Phys. Rev. Lett.* **85**, 4450 (2000).

[5] J. Colgan, M.S. Pindzola, and F. Robicheaux, *J. Phys. B: At. Mol. Opt. Phys.* **34**, L457 (2001).

[6] C.W. McCurdy, D.A. Horner, T.N. Resigno, and F. Martín, *Phys. Rev.* A **69**, 032707 (2004).

[7] S. Bellm, J. Lower, and K. Bartschat, *Phys. Rev. Lett.* **96**, 223201 (2006).

[8] S. Bellm, J. Lower, K. Bartschat, X. Guan, D. Weflen, M. Foster, A.L. Harris, and D.H. Madison, *Phys. Rev.* A **75**, 042704 (2007).

[9] C. Dupré, A. Lahmam-Bennani, A. Duguet, F. Mota-Furtado, P.F. O'Mahony, and C. Dal Cappello, *J. Phys. B: At. Mol. Opt. Phys.* **25**, 259 (1992).

[10] G. Sakhelashvili, A. Dorn, C. Hohr, J. Ullrich, A.S. Kheifets, J. Lower, and K. Bartschat, *Phys. Rev. Lett.* **95**, 033201 (2005).

[11] A.S. Kheifets, I. Bray, I.E. McCarthy, and B. Shang, *Phys. Rev.* A **50**, 4700 (1994).

[12] P.J. Marchalant, J. Rasch, C.T. Whelan, D.H. Madison, and H.R.J. Walters, *J. Phys. B: At. Mol. Opt. Phys.* **32**, L705 (1999).

[13] M. Dogan and A. Crowe, *J. Phys. B: At. Mol. Opt. Phys.* **33**, L461 (2000).

[14] A.L. Harris, M. Foster, C. Ryan-Anderson, J.L. Peacher, and D.H. Madison, *J. Phys. B: At. Mol. Opt. Phys.* **41**, 135203 (2008).

[15] V.V. Balashov and I.V. Bodrenko, *J. Phys. B: At. Mol. Opt. Phys.* **32**, L687 (1999).

[16] R.J. Tweed, *J. Phys. B: At. Mol. Opt. Phys.* **5**, 810 (1972).

[17] A. Franz and P.L. Altick, *J. Phys. B: At. Mol. Opt. Phys.* **25**, L257 (1992).

[18] B. Rouvellou, S. Rioual, A. Pochat, R.J. Tweed, J. Langlois, V.G. Nguyen, and O. Robaux, *J. Phys. B: At. Mol. Opt. Phys.* **33**, L599 (2000).

[19] A. Franz and P.L. Altick, *J. Phys. B: At. Mol. Opt. Phys.* **28**, 4639 (1995).

[20] Z. Chen and D.H. Madison, *J. Phys. B: At. Mol. Opt. Phys.* **38**, 4195 (2005).

[21] A.S. Kheifets, I. Bray, and K. Bartschat *J. Phys. B: At. Mol. Opt. Phys.* **32**, L433 (1999).

[22] P. J Marchalant, B. Rouvellou, J. Rasch, S. Rioual, C.T. Whelan, A. Pochat, D.H. Madison, and H.R.J. Walters, *J. Phys. B: At. Mol. Opt. Phys.* **33**, L749 (2000).

[23] Y. Fang and K. Bartschat, *J. Phys. B: At. Mol. Opt. Phys.* **34**, L19 (2001).

[24] L. Avaldi, R. Camilloni, R. Multari, G. Stefani, J. Langlois, O. Robaux, R.J. Tweed, and V.G. Nguyen, *J. Phys. B: At. Mol. Opt. Phys.* **31**, 2981 (1998).

[25] L. H. Thomas, *Proc. R. Soc. London* A **114**, 561 (1927).

[26] J. R. Oppenheimer, *Phys. Rev.* **31**, 349 (1928).

[27] D.R. Bates and A. Dalgarno, *Proc. Phys. Soc.* A **66**, 972 (1953).

[28] A. Dalgarno and H.N. Yadav, *Proc. Phys. Soc.* A **66**, 173 (1953).

[29] H. C. Brinkman and H. A. Kramers, *Proc. Acad. Sci. Amsterdam* **33**, 973 (1930).

[30] J. D. Jackson and H. Schiff, *Phys. Rev.* **89**, 359 (1953).

[31] D.R. Bates and A. Dalgarno, *Proc. Phys. Soc.* A **66**, 972 (1953).

[32] H. Schiff, *Can. J. Phys.* **32**, 393 (1954).

[33] T. Pradhan, *Phys. Rev.* **105**, 1250 (1957).

[34] Dž. Belkić and A. Salin, *J. Phys. B: At. Mol. Opt. Phys.* **11**, 3905 (1978).

[35] B. H. Bransden, A. Dalgarno, and N. M. King, *Proc. Phys. Soc.* A **67**, 1075 (1954).

[36] R. A. Mapleton, *Phys. Rev.* **130**, 1829 (1963).

[37] R. A. Mapleton, *Phys. Rev.* **130**, 1839 (1963).

[38] V. Malaviya, *J. Phys. B: At. Mol. Opt. Phys.* **2**, 843 (1969).

[39] H.K. Macomber and T.G. Webb, *Proc. Phys. Soc.* **92**, 839 (1967).

[40] R.H. Bassel and E. Gerjuoy, *Phys. Rev.* **117**, 749 (1960).

[41] K. Dettmann and G. Leibfried, *Z. Phys.* **218**, 1 (1969).

[42] A. Salin, *J. Phys. B: At. Mol. Opt. Phys.* **4**, L125 (1971).

[43] Dž. Belkić, *Physica Scripta* **47**, 18 (1993).

[44] M. Kimura, *J. Phys. B: At. Mol. Opt. Phys.* **21**, L19 (1988).

[45] Dž. Belkić, *J. Phys. B: At. Mol. Opt. Phys.* **26**, 497 (1993).

[46] M. Purkait, S. Sounda, A. Dhara, and C.R. Mandal, *Phys. Rev.* A **74**, 042723 (2006).

[47] M. Ghosh, A. Dhara, C.R. Mandal, and M. Purkait, *Phys. Rev.* A **78**, 042708 (2008).

[48] T.F. Tuan and E. Gerjuoy, *Phys. Rev.* **117**, 7856 (1960).

[49] R. Mapleton, *Phys. Rev.* **122**, 528 (1961).

[50] S.R. Rogers and J.H. McGuire, *J. Phys. B: At. Mol. Opt. Phys.* **13**, L497 (1977).

[51] Dž. Belkić and A. Salin, *J. Phys. B: At. Mol. Opt. Phys.* **11**, 3905 (1978).

[52] T.C. Theisen and J.H. McGuire, *Phys. Rev.* A **20**, 1406 (1979).

[53] R.D. Rivarola, R.D. Piacentini, A. Salin, and Dž. Belkić, *J. Phys. B: At. Mol. Opt. Phys.* **13**, 2601 (1980).

[54] R. Gayet, R.D. Rivarola, and A. Salin, *J. Phys. B: At. Mol. Opt. Phys.* **14**, 2421 (1981).

[55] T.S. Ho, D. Umberger, R.L. Day, M. Lieber, and F.T. Chan, *Phys. Rev.* A **24**, 705 (1981).

[56] S.K. Shrivastava, A. Kumar, and B.N. Roy, *J. Phys. B: At. Mol. Opt. Phys.* **16**, 215 (1983).

[57] R.D. Rivarola and A. Salin, *J. Phys. B: At. Mol. Opt. Phys.* **17**, 659 (1984).

[58] G. R. Deco, J.M. Maidagan, and R.D. Rivarola, *J. Phys. B: At. Mol. Opt. Phys.* **17**, L707 (1984).

[59] V.A. Sidorovich, V.S. Nikolaev, and J.H. McGuire, *Phys. Rev.* A **31**, 2193 (1985).

[60] G.C. Saha, S. Datta, and S.C. Mukherjee, *Phys. Rev.* A **34**, 2809 (1986).

[61] Dž. Belkić, *Phys. Rev.* A **37**, 55 (1988).

[62] N. Toshima and A. Igarashi, *Phys. Rev.* A **45**, 6313 (1992).

[63] I. Mančev, V. Mergel, and L. Schmidt, *J. Phys. B: At. Mol. Opt. Phys.* **36**, 2733 (2003).

[64] P.N. Abufager, A.E. Martínez, R.D. Rivarola, and P.D. Fainstein, *J. Phys. B: At. Mol. Opt. Phys.* **37**, 817 (2004).

[65] I. Mančev, *Phys. Rev.* A **60**, 351 (1999).

[66] P.N. Abufager, P.D. Fainstein, A.E. Martínez, and R.D. Rivarola, *J. Phys. B: At. Mol. Opt. Phys.* **38**, 11 (2005).

[67] D. Fischer, et. al, *Phys. Rev.* A **73**, 052713 (2006).

[68] D.S.F Crothers and R. McCarroll, *J. Phys. B: At. Mol. Opt. Phys.* **20**, 2835 (1987).

[69] F. Decker and J. Eichler, *J. Phys. B: At. Mol. Opt. Phys.* **22**, L95 (1989).

[70] Dž. Belkić and R.K Janev, *J. Phys. B: At. Mol. Opt. Phys.* **6**, 1020 (1973).

[71] Dž. Belkić and A. Salin, *J. Phys. B: At. Mol. Opt. Phys.* **9**, L397 (1976).

[72] P.T. Greenland, *J. Phys. B: At. Mol. Opt. Phys.* **14**, 3707 (1981).

[73] C.K. Tan and A.R. Lee, *J. Phys. B: At. Mol. Opt. Phys.* **14**, 2409 (1981).

[74] H. Ryufuku and T. Watanabe, *Phys. Rev.* A **18**, 2005 (1978).

[75] H. Ryufuku and T. Watanabe, *Phys. Rev.* A **19**, 1538 (1979).

[76] N. Toshima, T. Ishihara, and J. Eichler, *Phys. Rev.* A **36**, 2659 (1987).

[77] D.P. Dewangan and J. Eichler, *J. Phys. B: At. Mol. Opt. Phys.* **18**, L65 (1985).

[78] H. Vogt, R. Schuch, E. Justiniano, M. Schulz, and W. Schwab, *Phys. Rev.* A **57**, 2256 (1986).

[79] S. Alston, *Phys. Rev.* A **38**, 3124 (1988).

[80] Dž. Belkić, R. Gayet, J. Hanssen, and A. Salin, *J. Phys. B: At. Mol. Opt. Phys.* **19**, 2945 (1986).

[81] Dž. Belkić, H.S. Taylor, *Phys. Rev.* A **35**, 1991 (1987).

[82] Dž. Belkić, S. Saini, and H.S. Taylor, *Phys. Rev.* A **36**, 1601 (1987).

[83] S.K. Datta, D.S.F. Crothers, and R. McCarroll, *J. Phys. B: At. Mol. Opt. Phys.* **23**, 479 (1990).

[84] K.M. Dunseath, D.S.F. Crothers, and T. Ishihara, *J. Phys. B: At. Mol. Opt. Phys.* **21**, L461 (1988).

[85] I. Mančev, *J. Phys. B: At. Mol. Opt. Phys.* **36**, 93 (2003).

[86] C. Sinha, S. Mukherjee, and N.C. Sil, *J. Phys. B: At. Mol. Opt. Phys.* **12**, 1391 (1979).

[87] S. Datta and S.C. Mukherjee, *J. Phys. B: At. Mol. Opt. Phys.* **13**, 539 (1980).

[88] C.R. Mandal, S. Datta, and S.C. Mukherjee, *Phys. Rev.* A **24**, 3044 (1981).

[89] K. Dettmann and G. Leibfried, *Phys. Rev.* **148**, 1271 (1966).

[90] P.J. Kramer, *Phys. Rev.* A **6**, 2125 (1972).

[91] R. Shakeshaft and L. Spruch, *Phys. Rev.* A **8**, 206 (1973).

[92] K. Omidvar, *Phys. Rev.* A **12**, 911 (1975).

[93] G. Lapicki and W. Losonsky, *Phys. Rev.* A **15**, 896 (1977).

[94] J.S. Briggs and L. Dubé, *J. Phys. B: At. Mol. Opt. Phys.* **13**, 771 (1980).

[95] R. Shakeshaft, *Phys. Rev. Lett.* **44**, 442 (1980).

[96] J.M. Wadehra, R. Shakeshaft, and J.H. Macek, *J. Phys. B: At. Mol. Opt. Phys.* **14**, L767 (1981).

[97] P.R. Simony and J.H. McGuire, *J. Phys. B: At. Mol. Opt. Phys.* **14**, L737 (1981).

[98] P.R. Simony, J.H. McGuire, and J. Eichler, *Phys. Rev.* A **26**, 1337 (1982).

[99] J. Macek and S. Alston, *Phys. Rev.* A **26**, 250 (1982).

[100] J.H. McGuire, P.R. Simony, O.L. Weaver, and J. Macek, *Phys. Rev.* A **26**, 1109 (1982).

[101] J.H. McGuire, J. Eichler, and P.R. Simony, *Phys. Rev.* A **28**, 2104 (1983).

[102] D.P. Dewangan and B.H. Bransden, *J. Phys. B: At. Mol. Opt. Phys.* **21**, L353 (1988).

[103] Dž. Belkić, *Phys. Rev.* A **43**, 4751 (1991).

[104] J.E. Miraglia, R.D. Piacentini, R.D. Rivarola, and A. Salin, *J. Phys. B: At. Mol. Opt. Phys.* **14**, L197 (1981).

[105] R. Hippler, S. Datz, P.D. Miller, P.L. Pepmiller, and P.F. Dittner, *Phys. Rev.* A **35**, 585 (1987).

[106] A.E. Martínez, R. Gayet, J. Hanssen, R.D. Rivarola, *J. Phys. B: At. Mol. Opt. Phys.* **27**, L375 (1994).

[107] R. Gayet, J. Hanssen, L. Jacqui, A. Martínez, R. Rivarola, *Physica Scripta* **53**, 549 (1996).

[108] S. Ghosh, A. Dhara, C.R. Mandal, M. Purkait, *Phys. Rev.* A **78**, 042708 (2008).

[109] Dž. Belkić, *Phys. Rev.* A **47**, 189 (1993).

[110] R. Gayet, R.D. Rivarola, A. Salin, *J. Phys. B: At. Mol. Opt. Phys.* **14**, 2421 (1981).

[111] R. Schuch, E. Justiniano, H. Vogt, G. Deco, and N. Gruen, *J. Phys. B: At. Mol. Opt. Phys.* **24**, L133 (1991).

[112] B. Bhattacharjee, M. Das, N.C. Deb, and S.C. Mukherjee, *Phys. Rev.* A **54**, 2973 (1996).

[113] M.S. Gravielle and J.E. Miraglia, *Phys. Rev.* A **45**, 2965 (1992).

[114] Dž. Belkić, *Phys. Rev.* A **47**, 3824 (1993).

[115] M.H. Mittleman, *Phys. Rev.* **122**, 499 (1961).

[116] T.B. Day, L.S. Rodberg, G.A. Snow, and J. Sucher, *Phys. Rev.* **123**, 1051 (1961).

[117] R.A. Mapleton, *Phys. Rev.* **126**, 1477 (1962).

[118] T. Pradhan and D.N. Tripathy, *Phys. Rev.* **130**, 2317 (1963).

[119] R.M. May, *Phys. Rev.* **136**, A669 (1964).

[120] J.R. Hiskes, *Phys. Rev.* **137**, A361 (1965).

[121] K. Omidvar, *Phys. Rev.* **153**, 121 (1967).

[122] S. Geltman, *J. Phys. B: At. Mol. Opt. Phys.* **4**, 1288 (1971).

[123] J.C.Y. Chen and P.J. Kramer, *Phys. Rev.* A **5**, 1207 (1972).

[124] Y.B. Band, *Phys. Rev.* A **8**, 243 (1973).

[125] Y.B. Band, *Phys. Rev.* A **8**, 2857 (1973).

[126] D. Rapp, *J. Chem. Phys.* **58**, 2043 (1973).

[127] J. Chaudhuri, A.S. Ghosh, and N.C. Sil, *Phys. Rev.* A **7**, 1544 (1973).

[128] J.S. Briggs and K. Dettmann, *Phys. Rev. Lett.* **33**, 1123 (1974).

[129] N.C. Sil, J. Chaudhuri, and A.S. Ghosh, *Phys. Rev.* A **12**, 785 (1975).

[130] K. Omidvar, J.E. Golden, and J.H. McGuire, *Phys. Rev.* A **13**, 500 (1976).

[131] R.E. Olson, A. Salop, R.A. Phaneuf, and F.W. Meyer, *Phys. Rev.* A **16**, 1867 (1977).

[132] R.E. Olson and A. Salop *Phys. Rev.* A **16**, 531 (1977).

[133] Dž. Belkić and R. Gayet, *J. Phys. B: At. Mol. Opt. Phys.* **10**, 1923 (1977).

[134] Dž. Belkić and R. Gayet, *J. Phys. B: At. Mol. Opt. Phys.* **10**, 1911 (1977).

[135] Dž. Belkić, *J. Phys. B: At. Mol. Opt. Phys.* **10**, 3491 (1977).

[136] J.S. Briggs, *J. Phys. B: At. Mol. Opt. Phys.* **10**, 3075 (1977).

[137] R. Shakeshaft and L. Spruch, *J. Phys. B: At. Mol. Opt. Phys.* **11**, L457 (1978).

[138] J.E. Golden, J.H. McGuire, and K. Omidvar, *Phys. Rev.* A **18**, 2373 (1978).

[139] F.T. Chan and J. Eichler, *Phys. Rev. Lett.* **42**, 58 (1979).

[140] S. Mukherjee, N.C. Sil, and D. Basu, *J. Phys. B: At. Mol. Opt. Phys.* **12**, 1259 (1979).

[141] J. Eichler and F.T. Chan, *Phys. Rev.* A **20**, 104 (1979).

[142] F.T. Chan and J. Eichler, *Phys. Rev.* A **20**, 1841 (1979).

[143] J.S. Briggs and K. Taulberg, *J. Phys. B: At. Mol. Opt. Phys.* **12**, 2565 (1979).

[144] C.D. Lin and L.N. Tunnell, *J. Phys. B: At. Mol. Opt. Phys.* **12**, L485 (1979).

[145] T.S. Ho, M. Lieber, F.T. Chan, and K. Omidvar, *Phys. Rev.* A **24**, 2933 (1981).

[146] J.K.M. Eichler, *Phys. Rev.* A **23**, 498 (1981).

[147] P.J. Martin, et. al *Phys. Rev.* A **23**, 2858 (1981).

[148] M. Kimura and W.R. Thorson, *Phys. Rev.* A **24**, 1780 (1981).

[149] J.H. McGuire, P.R. Simony, O.L. Weaver, and J. Macek, *Phys. Rev.* A **26**, 1109 (1982).

[150] J.M. Maidagan and R.D. Rivarola, *J. Phys. B: At. Mol. Opt. Phys.* **17**, 2477 (1984).

[151] D.S.F. Crothers and K.M. Dunseath, *J. Phys. B: At. Mol. Opt. Phys.* **20**, 4115 (1987).

[152] H. Bachau, G. Deco, and A. Salin, *J. Phys. B: At. Mol. Opt. Phys.* **21**, 1403 (1988).

[153] N.V. deCastro Faria, F.L. Freire, Jr., and A.G. de Pinho, *Phys. Rev.* A **37**, 280 (1988).

[154] N.C. Deb and D.S.F. Crothers, *J. Phys. B: At. Mol. Opt. Phys.* **22**, 3725 (1989).

[155] I. Mančev, *Physica Scripta* **51**, 762 (1994).

[156] H.A. Slim, E.L. Heck, B.H. Bransden, and D.R. Flower, *J. Phys. B: At. Mol. Opt. Phys.* **24**, 2353 (1991).

[157] Dž. Belkić, *Phys. Rev.* A **43**, 4751 (1991).

[158] L.F. Errea, C.Harel, H. Jouin, J.M. Maidagan, L. Méndez, B. Pons, and A. Riera, *Phys. Rev.* A **46**, 5617 (1992).

[159] H.F. Busnengo, A.E. Martínez, and R.D. Rivarola, *Physica Scripta* **51**, 190 (1994).

[160] L.F. Errea, J.D. Gorfinkiel, C. Harel, H. Jouin, A. Macias, L. Méndez, B. Pons, and A. Riera, *Physica Scripta* **T62**, 27 (1996).

[161] H.F. Busnego, A.E. Martínez, and R.D. Rivarola, *J. Phys. B: At. Mol. Opt. Phys.* **29**, 4193 (1996).

[162] L.F. Errea, C. Harel, J. Jouin, L. Mendez, B. Pons, and A. Riera, *J. Phys. B: At. Mol. Opt. Phys.* **31**, 3527 (1998).

[163] L. Gulyas, P.D. Fainstein, and T. Shirai, *Phys. Rev.* A **65**, 052720 (2002).

[164] Dž. Belkić, R. Gayet, J. Hanssen, I. Mančev, and A. Nunez, *Phys. Rev.* A **56**, 3675 (1997).

[165] M. Ghosh, C.R. Mandal, and S.C. Mukherjee, *J. Phys. B: At. Mol. Opt. Phys.* **18**, 3797 (1985).

[166] D.P. Dewangan and J. Eichler, *J. Phys. B: At. Mol. Opt. Phys.* **19**, 2939 (1986).

[167] M.S. Schöffler, J. Titze, L.Ph.H. Schmidt, T. Jahnke, N. Neumann, O. Jagutzki, H. Schmidt-Böcking, R. Dörner, and I. Mančev, *Phys. Rev.* A **79**, 064701 (2009).

[168] A. Hasan, B. Tooke, M. Zapukhlyak, T. Kirchner, and M. Schulz, *Phys. Rev.* A **74**, 032703 (2006).

[169] M. Zapukhlyak, T. Kirchner, A. Hasan, B. Tooke, and M. Schulz, *Phys. Rev.* A **77**, 012720 (2008).

[170] J.H. McGuire and L. Weaver, *Phys. Rev.* A **16**, 41 (1977).

[171] K.M. Dunseath and D.S.F. Crothers, *J. Phys. B: At. Mol. Opt. Phys.* **24**, 5003 (1991).

[172] M. Schulz, T. Vajnai, and J.A. Brand, *Phys. Rev.* A **75**, 022717 (2007).

[173] H. Martinez, F.B. Alarcon, and A. Amaya-Tapia, *Phys. Rev* A **78**, 062715 (2008).

[174] V.V. Afrosimov, R.N. Ilin, and E.S. Solovev, *Sov. Phys. Tech. Phys.* **5**, 661 (1960).

[175] C.J. Joachain, *Quantum Collision Theory*, New York: North-Holland, (1975).

[176] J.F. Hart and G. Herzberg, *Phys. Rev.* **106**, 79 (1957).

[177] M. Gell-Mann and M.L. Goldberger, *Phys. Rev.* **91**, 398 (1953).

[178] S. Jones and D.H. Madison, *J. Phys. B: At. Mol. Opt. Phys.* **27**, 1423 (1994).

[179] S. Jones and D.H. Madison, *Phys. Rev.* A **62**, 042701 (2000).

[180] D.H. Madison, D. Fischer, M. Foster, M. Schulz, R. Moshammer, S. Jones and J. Ullrich, *Phys. Rev. Lett.* **91**, 253201 (2003).

[181] V.E. Bubelev and D.H. Madison, *J. Phys. B: At. Mol. Opt. Phys.* **26**, 3541 (1993).

[182] M.R.C. McDowell and J.P. Coleman, *Introduction to the Theory of Ion-Atom Collisions*, (North-Holland, 1970).

[183] D.S.F. Crothers and J.F. McCann, *J. Phys. B: At. Mol. Opt. Phys.* **16**, 3229 (1983).

[184] F.W. Byron and C.J. Joachain *Phys. Rev.* **146**, 1 (1966).

[185] S. Chandrasekhar, *Rev. Mod. Phys.* **16**, 301 (1944).

[186] S. Bellm, J. Lower, E. Weigold, I. Bray, D.V. Fursa, K. Bartschat, A.L. Harris, and D.H. Madison, *Phys. Rev.* A **78**, 032710 (2008).

[187] D.H. Madison, M. Schulz, S. Jones, M. Foster, R. Moshammer, and J. Ullrich, *J. Phys. B: At. Mol. Opt. Phys.* **35**, 3297 (2002).

[188] K. Bartschat, I. Bray, D.V. Fursa, and A.T. Stelbovics, *Phys. Rev.* A **76**, 024703 (2007).

[189] Y.B. Band, *Phys. Rev.* A **8**, 2857 (1973).

[190] N.C. Sil, B.C. Saha, H.P. Saha, and P. Mandal, *Phys. Rev.* A **19**, 655 (1979).

VITA

Allison Lynn Harris was born in Springfield, Missouri on June 8, 1983. She grew up in Branson, Missouri, and graduated from Branson High School in 2001. In December, 2004, she graduated Summa Cum Laude from Drury University with a Bachelor of Arts degree in Physics, and Minors in Mathematics and Global Studies. In January, 2005, she enrolled at the University of Missouri-Rolla (now Missouri University of Science and Technology) with a Chancellor's Fellowship, and began work on her PhD in Physics.

While at Missouri S&T, she published four peer-reviewed articles, and presented research at eight national and international conferences. She was an invited speaker at the 2009 International Symposium on (e,2e), Double Photoionization and Related Topics & 15th Int'l Symposium on Polarization and Correlation in Electronic and Atomic Collisions.

She was the 2006 winner, and 2007 co-winner, of the Schearer Prize competition. She also received second place in the 2007 Missouri S&T/University of Missouri-St. Louis physics graduate student poster competition. She served as the Physics Department representative, and Treasurer, for the Council of Graduate Students, and received the 2008 Council of Graduate Students Distinguished Services Award.